



Norwegian University of  
Science and Technology

# Head losses and flow field at trash racks

**Eirik Bruvik Øvregård**

Civil and Environmental Engineering

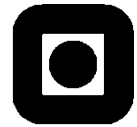
Submission date: June 2016

Supervisor: Jochen Aberle, IVM

Co-supervisor: Christy Ushanth Navaratnam, IVM  
Marcell Szabo-Meszaros, IVM

Norwegian University of Science and Technology  
Department of Hydraulic and Environmental Engineering





## MASTEROPPGAVE

Student: Eirik Øvregård

Title: Head losses and flow field at trash racks

### 1 BACKGROUND

Norway's electric energy demand is almost exclusively met by hydropower which will remain the most important energy source for the foreseeable future due to Norway's unique topography, climate and availability of natural reservoirs. However, upcoming revision of hydropower licenses, implementation of the European Water Framework Directive (WFD) and new national legislations (The Nature Diversity Act) exerts pressures on the industry by establishing targets for improved environmental conditions in regulated rivers, potentially at the cost of power production. In fact, river fragmentation due to the presence of hydropower structures (dam, weirs) is a ubiquitous occurrence in many rivers which are used as migratory routes by migrating fish. Maintaining or re-establishing longitudinal and lateral connectivity for fish in fragmented rivers is pointed out as important in the revisions of hydropower licenses and is crucial to achieve WFD's target. Given the imminent need for developing efficient downstream passage systems which minimize the risk of injury and mortality associated with fish passage through hydropower stations in the hydropower industry in Norway, the scientific approach to downstream migration solutions in Norway is imperative and is presently developed within the CEDREN-project SAFEPASS. A work package within SAFEPASS focuses exclusively on the effectivity of physical barriers such as trash-racks and screens in order to prevent migrating fish from entering turbines. However, head losses due to narrow bar spacing and species specific responses call for improved designs of fish protection systems. For this purpose, different bar racks and optimal repelling methods varying from larger bar spacing through angled rack designs to solutions with horizontal bars will be tested experimentally in the research project. The main purpose of the experiments is to study the head losses associated with the different trash-rack setups as well as the characteristics of the turbulent flow field near the trash-rack.

## **2 TASKS**

The objective of the present MSc-thesis is to carry out experiments in a hydraulic model at the NTNU hydraulic laboratory in order to determine the head losses and turbulent flow field associated with different trash-rack designs. The trash-rack designs and experimental boundary conditions will be defined through the SAFEPASS project. The measurements related to the turbulent flow field should be carried out with Particle Image Velocimetry (PIV) to guarantee a high temporal and spatial resolution.

In order to fulfil the objectives, the MSc-thesis should cover the following issues:

1. Literature review on head losses and the turbulent flow field at trash racks with special focus on recent developments
2. Description of the (given) experimental setup
3. Design of the experimental setup for the instrumentation required to measure head losses and turbulent flow field
4. Execution of experiments for at least three different trash-rack setups for given boundary conditions
5. Determination of head-losses and visualisation of the turbulent flow field in the vicinity of the bars
6. Discussion of results
7. Recommendations for future investigations

Discussions with the supervisor will be used to refine details of the experimental setup and the experimental procedure.

## **3 SUPERVISION AND DATA**

Professor Jochen Aberle from NTNU will be main-supervisor of the project work. Co-supervisors will be MSc Christy Ushanth Navaratnam and MSc Marcell Szabo-Meszaros. Discussions and input from colleagues and other researchers at NTNU, NVE, SINTEF, NINA etc. is recommended. Significant inputs from others shall, however, be referenced in an adequate manner.

The research and engineering work carried out by the candidate in connection with this thesis shall remain within an educational context.

Other contact persons available for technical support: Geir Tesaker, NTNU

## **4 REPORT FORMAT AND REFERENCE STATEMENT**

The MSc-thesis shall be typed by a word processor and figures, tables, photos etc. shall be of good report quality. The report shall include a summary of not more than 450 words that is suitable for electronic reporting, a table of content, lists of figures and tables, a list of literature and other relevant references and a signed statement where the candidate states that the presented work is his own and that significant outside input is identified and referred. The report shall have a professional structure, assuming professional senior engineers (not in teaching or research) as the main target group. The thesis should be submitted in pdf-form in DAIM and in the form of three hardcopies that should be sent to the supervisor/department via the printing shop. The thesis should not be delivered later than Friday, June 10, 2016.

Trondheim, 14. januar 2016

---

Jochen Aberle  
Professor

## **Abstract**

The purpose of this master thesis was to measure the head loss caused by fish-friendly trash racks in an open water channel and to measure the turbulent flow field around its bars. Angled model trash racks with different bar arrangement and orientation were tested, accompanied by a bypass. As a part of the master thesis a literature review was done with special focus on the turbulent flow field around bars and on different equations used for head loss prediction. Experiments were carried out at the NTNU hydraulic laboratory in a straight open channel. Head loss measurements were carried out for six racks at six different discharges. The measurements related to the turbulent flow field were carried out by the V3V PIV system from TSI Inc. in vicinity of the bars downstream and upstream of the trash racks. The results showed that horizontally barred racks overall performed better than trash racks with vertical streamwise and inclined bars with regards to head loss. The results also provide detailed volumetric velocity distribution plots in vicinity of the bars. Head loss predictions were made on the basis of several head loss equations. The head loss equations were able to predict the actual head losses to a certain degree, but further studies are needed to fully determine the effects of angled trash racks and bypasses on head losses. Further studies on trash racks with horizontal bars are also suggested.

## Sammendrag

Formålet med denne masteroppgaven var å måle falltapet over fiskevennlige varegrinder, og å måle det turbulente strømningsfeltet i nærheten av stavene i grinden. Vinklede varegrindmodeller med forskjellige stavformer og orientering ble testet. Forsøkene inneholdt også en forbistrømningskanal (bypass). Som en del av masteroppgaven ble det gjort et litteraturstudie med spesielt fokus på turbulente strømningsfelt rundt staver, og på falltapsformler som senere skulle brukes til å anslå falltapene over varegrindene. Forsøket ble utført i vassdragslaboratoriet ved NTNU. Falltapsmålingene ble utført for seks forskjellige varegrinder ved seks forskjellige vannføringer. Målingene relatert til turbulente strømningsfelt ble gjennomført av V3V PIV-systemet fra TSI Inc. i nærheten av stavene nedstrøms og oppstrøms for varegrindene. Resultatene viste at varegrinder med horisontale staver gav bedre resultater med tanke på falltap enn varegrinder med vertikale staver. Resultatene viser også detaljerte figurer som viser den volumetriske hastighetsfordelingen i nærheten av stavene. Falltapene ble også anslått ved hjelp av en rekke falltapsligninger. Falltapsligningen var i stand til å anslå brukbare verdier, men videre studier er nødvendige for å fullt fastslå effekten av vinklede varegrinder, sammen med en forbistrømningskanal, har på falltap. Videre undersøkelser på varegrinder med horisontale staver er også anbefalt.

## **Preface**

This Master Thesis signifies the end of my five years as a student at NTNU. It also signifies the end of a challenging, but very interesting and highly educational last semester.

I would like to thank my supervisor Jochen Aberle, for his help and flexibility during this process. I would also like to give a special thanks to co-supervisors Christy Ushanth Navaratnam and Marcell Szabo-Meszaros for their help and company during the many hours in the hydraulics laboratory, and for their help piecing it all together after the experiment.

Trondheim 10<sup>th</sup> of June

---

Eirik Øvregård

# Table of Contents

List of Figures .....	X
List of Tables.....	XI
Abbreviations .....	XII
List of Symbols .....	XIII
<b>1 INTRODUCTION.....</b>	<b>1</b>
<b>2 HEAD LOSSES AND TURBULENT FLOW FIELD AT TRASH RACKS.....</b>	<b>3</b>
2.1 Flow field at trash racks.....	3
2.2 Head loss calculation.....	4
2.3 Applicability of the head loss equations.....	7
2.4 Difficulties regarding trash racks and downstream migration of fish .....	8
<b>3 METHODOLOGY.....</b>	<b>9</b>
3.1 Experimental setup.....	9
3.1.1 Flume and boundary conditions .....	9
3.1.2 Trash racks and bypass .....	9
3.1.3 Head loss measurements .....	12
3.1.4 Particle Image Velocimetry .....	12
3.2 Experimental procedure .....	14
<b>4 RESULTS .....</b>	<b>16</b>
4.1 Head loss and head loss coefficients .....	16
4.1.1 Kirschmer-Mosonyi (1966).....	19
4.1.2 Meusburger (2002).....	19
4.1.3 Clark et al. (2010).....	19
4.1.4 Raynal et al. (2013b).....	20
4.1.5 Raynal et al. (2013a).....	20
4.2 V3V results .....	22
4.2.1 Downstream measurements.....	23
4.2.2 Upstream measurements .....	26
<b>5 DISCUSSION AND CONCLUSION.....</b>	<b>28</b>
5.1 Measured water level and head loss .....	28
5.2 Predicted head loss .....	29

5.3	Flow field in the vicinity of the bars .....	30
5.4	Conclusions and further investigation.....	31
<b>6</b>	<b>REFERENCES .....</b>	<b>32</b>

## List of Figures

Figure 2.1: Flow pattern past a square illustrating separation at the edges.....	3
Figure 2.2: Effects of inclined bars on turbulence level and vortex generation.....	4
Figure 2.3: Plan view of the experimental setup of Meusburger (2002) and Clark et al.(2010).....	6
Figure 2.4: Plan view of experimental setup by Raynal et al. (2014).....	7
Figure 3.1: Armfield Ltd flume used in this experiment.....	9
Figure 3.2: Plan view of the rack and the bypass .....	10
Figure 3.3: Side view of the rack and by pass.....	10
Figure 3.4: Plan view of sections of the rack and bypass .....	10
Figure 3.5: Front view of rack I-VI.....	11
Figure 3.6: Bar shapes with values in mm.....	11
Figure 3.7: Piezometer layout.....	12
Figure 3.8: Concept of a "Triplet" in V3V .....	13
Figure 3.9: The measurement area just downstream of the rack.....	14
Figure 3.10: Picture of the rack, laser and V3V camera probe .....	15
Figure 4.1: Water surface visualisation for Rack I-VI. ....	16
Figure 4.2: Measured head losses for all racks and discharges.....	21
Figure 4.3: Comparison of predicted and measured head loss $\Delta h$ at $Q = 170$ l/s.....	21
Figure 4.4: Example of V3V isometric velocity plot with vertical bar placement.....	22
Figure 4.5: Example of V3V isometric velocity plot with horizontal bar placement.....	22
Figure 4.6: Example of top view velocity plot with vertical bar placement.....	23
Figure 4.7: Example of side view velocity plot with horizontal bar placement .....	23
Figure 4.8: Isometric projection of velocity magnitude distribution for Rack I-II and Rack V-VI at $Q = 170$ l/s downstream of the rack.....	24
Figure 4.9: Top view velocity magnitude distribution for Rack I-IV and front view of Rack V-VI at $Q = 170$ l/s downstream of the rack.....	25
Figure 4.10: Isometric projection of velocity magnitude distribution for Rack II, Rack IV and Rack VI at $Q = 170$ l/s upstream of the rack.....	26
Figure 4.11: Top view velocity magnitude distribution for Rack II, Rack IV and Rack VI at $Q = 170$ l/s upstream of the rack .....	27

## List of Tables

Table 2.1: Comparison of max. and min. values of $\alpha$ and $e/b$ in different studies .....	8
Table 3.1: Description of trash racks .....	11
Table 3.2: Piezometer layout. Distance is from the inlet. ....	12
Table 4.1: Friction head loss $\Delta H_0$ between $H_2$ and $H_4$ at different discharges .....	17
Table 4.2: Discharge through the bypass for each rack at a given total discharge. ....	17
Table 4.3: Velocity data sorted by rack and discharge .....	18
Table 4.4: Calculated head loss $\Delta H$ [mm] from measured data.....	18
Table 4.5: Kirschmer-Mosonyi - calculated head loss coefficients .....	19
Table 4.6: Meusbürger - calculated head loss coefficients.....	19
Table 4.7: Clark et al. (2010) - calculated head loss coefficients.....	20
Table 4.8: Raynal et al. (2013b) - calculated head loss coefficients.....	20
Table 4.9: Raynal et al. (2013a) - calculated head loss coefficients.....	20
Table 4.10: Predicted head loss coefficients $\xi$ .....	20

## Abbreviations

---

<b>2D, 3D</b>	Two-dimensional, three-dimensional
<b>CSV</b>	Comma Separated Value
<b>PIV</b>	Particle Image Velocimetry
<b>V3V</b>	Volumetric 3-component Velocimetry

---

## List of Symbols

Symbol	Unit	Description
$A$	$m^2$	The cross sectional area of flow
$b$	$m$	Bar thickness
$B$	$m$	Width of the flume minus the width of the bypass
$B_r$	$m$	Width of the face of the trash rack
$e$	$m$	Clear space between two bars
$g$	$m/s^2$	Gravitational acceleration
$H_i$	$m$	Water depth at a certain piezometer
$k_F, k_b, K_i$	-	Bar shape factors
$k_v$	-	Debris blockage factor
$k\delta$	-	Oblique flow factor
$n$	-	Number of bars in a rack
$O_g, P, \eta$	-	Blockage ratio
$p$	$m$	Bar depth
$Q$	$m^3/s$	Discharge
$R_b$	-	Bar Reynolds number
$U$	$m/s$	Flow velocity
$V_i$	$m/s$	Velocity at a certain piezometer along x
$x, y, z$	$m$	Axes dimensions
$\alpha$	$^\circ$	Trash rack angle from the wall of the flume
$\theta$	$^\circ$	Vertical inclination of the bar relative to the floor
$\delta$	$^\circ$	Angle between the bars and the flow
$\Delta H$	$m$	Head loss due to the rack
$\Delta H_0$	$m$	Head loss due to the friction in the flume
$\lambda$	$nm$	Laser wavelength
$\nu$	$kg/(s \cdot m)$	Viscosity
$\xi$	-	Head loss coefficient

# 1 Introduction

Trash racks installed at intakes for hydroelectric power plants are used to prevent floating and submerged debris from causing damage and operational problems to downstream structures like turbines and conveyance system. Trash racks also serves to prevent fish e.g. silver eel (*Anguilla Anguilla*) and smolts from entering the water conveyance system and turbines. Trash racks will however cause unfavourable flow conditions and energy dissipation. This energy dissipation is called head loss as it reduces the hydraulic head, and consequently the hydroelectric power plants' energy output. Head loss is therefore a key parameter in designing trash racks.

Hydraulic head loss depends largely on the geometry of the trash rack and the bars. Most experimental studies focus on bar shape, bar size, spacing, blockage ratio and the angle of the approaching flow to estimate head loss. The blockage ratio, defined as area of the bars divided by total rack area, is arguably the most important factor in designing trash racks. Large spacing between the bars can result in reduced energy losses, while smaller spacing between the bars will physically prevent more debris and fish to enter the intake at the cost of increased head loss. The shape of the bars and the angle of approaching flow also plays an integral part in defining the turbulent flow fields around the bars.

Trash racks has typically been designed by finding the “sweet spot” between geometry and the cost of making and maintaining it. More precisely the relationship between production losses due to head loss, and the cost of constructing and cleaning the rack. However, due to the decline of smolts and silver eels in European watercourses (Dekker, 2003), new designs of trash racks might be required to take fish and eel migration into account. European Council regulation no. 1100/2007 (EC, 2007) dictates that eel mortality due to anthropogenic factors should be reduced to a minimum. Turbines and trash racks pose a large threat to fish and eel in their downstream migration due to individuals passing through the trash rack and passing through turbines, or injure themselves on the rack itself (Travade et al., 2010). This have resulted in an increased focus on reducing fish mortality caused by hydroelectric power plant structures.

SafePass is a project by CEDREN (Centre for Environmental Design of Renewable Energy) which seeks “safe and efficient two-way migration for salmonids and European eel past hydropower structures” (Cedren.no, 2016). Both downstream and upstream migration solutions will result in water loss and production loss on hydro power plants. The project aims at finding the best solution for guiding fish and eel downstream, without crippling the hydropower plants from producing energy. This experiment is embedded in the SafePass project.

Solutions like electrical production stop during fish and eel migration, and fish friendly turbines have been proposed. However, stopping production during migration will be far to costly and the fish friendly turbines are as of now only efficient for limited head discharge ranges (Raynal et al. (2013a)). Altering trash rack designs to be more fish friendly is therefore a highly acceptable solution. Fish friendly trash racks typically have reduced spacing between the bars to prevent smaller fish from entering the conveyance system. This will on the other hand increase the head loss through the trash rack. A solution is to guide the fish by the use of angled racks towards a bypass, leaving the fish unharmed (O’Keefe and Tumpenny, 2005).

The object of this thesis is to carry out experiments in a hydraulic model at the NTNU (Norwegian University of Science and Technology) hydraulics laboratory in order to determine the head losses and turbulent flow field associated with different angled trash rack designs. Head loss measurements will be done for six trash racks at six different discharges. The measurements related to the turbulent flow field will be carried out with Volumetric 3-Component Velocimetry

(V3V), a novel three-dimensional PIV system by TSI Inc. The head loss and turbulent flow field results for each trash rack will be presented and compared to each other. The results will also be evaluated in terms of fish-friendliness, with the boundary conditions set by former studies. However, this is first and foremost a study from a hydraulics point of view, and will therefore focus mainly on the head loss and turbulent flow field measurements.

## 2 Head losses and turbulent flow field at trash racks

### 2.1 Flow field at trash racks

Trash racks represent an obstruction the flow has to pass. The bars in the trash rack reduces the cross sectional area and forces the flow to accelerate through the gaps in the trash rack. This acceleration causes increased velocity and shear stress along the bars. Due to viscous effects a thin layer called the boundary layer forms next to the surface. The boundary layer is the layer between the surface of an object, where the velocity is zero, and the flow. If the fluid in the inner part of the boundary layer travels far enough against an adverse pressure gradient, the fluid may slow down to zero velocity. When this happens the boundary layer separates from the object and a wake develops behind the object. This is called the separation point. The separation creates a reverse flow region which is highly turbulent and unsteady, shedding vortices and eddies that dissipate energy (Crowe et al. 2010). This phenomenon is shown in Figure 2.1, where the separation point is at the vertical edges.

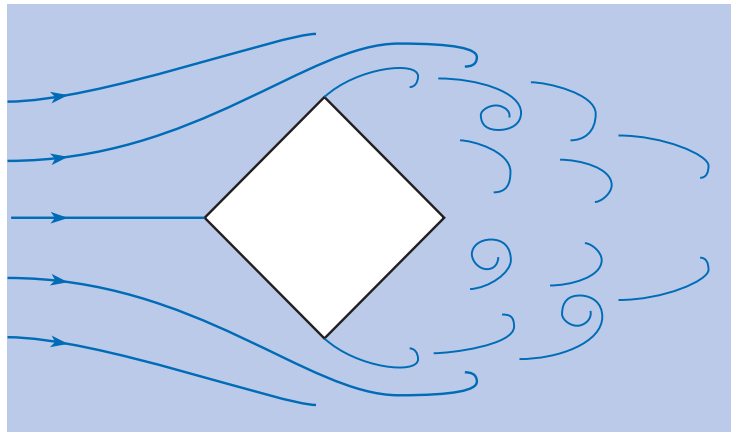


Figure 2.1: Flow pattern past a square illustrating separation at the edges (Crowe et al. (2010), p. 112)

Bar geometry (i.e. bar shape, streamwise bar depth and bar thickness) plays a large role in defining the head loss. The relationship between the streamwise bar depth  $p$  and the bar thickness  $b$  plays a big part when it comes to energy dissipation. Osborn (1968) observed that head loss trash racks rectangular bars decreased as  $b/p$  increased from 1 to 3. For short bars ( $p/b < 3$ ) the boundary layer separation occurred near the leading edge of the bars and did not reattach to the bars within the depth of the bars, shedding vortices downstream of the bars. For long bars ( $p/b > 3$ ) the separated flow reattached to the sides within the depth of the bars. It was argued that as the bar depth increases a greater area of the wake cavity is occupied by the bars reducing the energy dissipation and subsequent head loss. Bars with hydrodynamic surfaces delays the point of boundary layer separation and further reduces the energy loss.

The bar inclination (angle between flow and bars) also influence the head loss. Tsikata et al. (2009) argued that the shear layer and vortex formation depend strongly on the bar inclination. Increased bar inclination tends to increase the velocity and turbulence level, and creates larger vortices closer to the leading edge on the leeward side. As a consequence, increased bar inclination results in increased head losses.

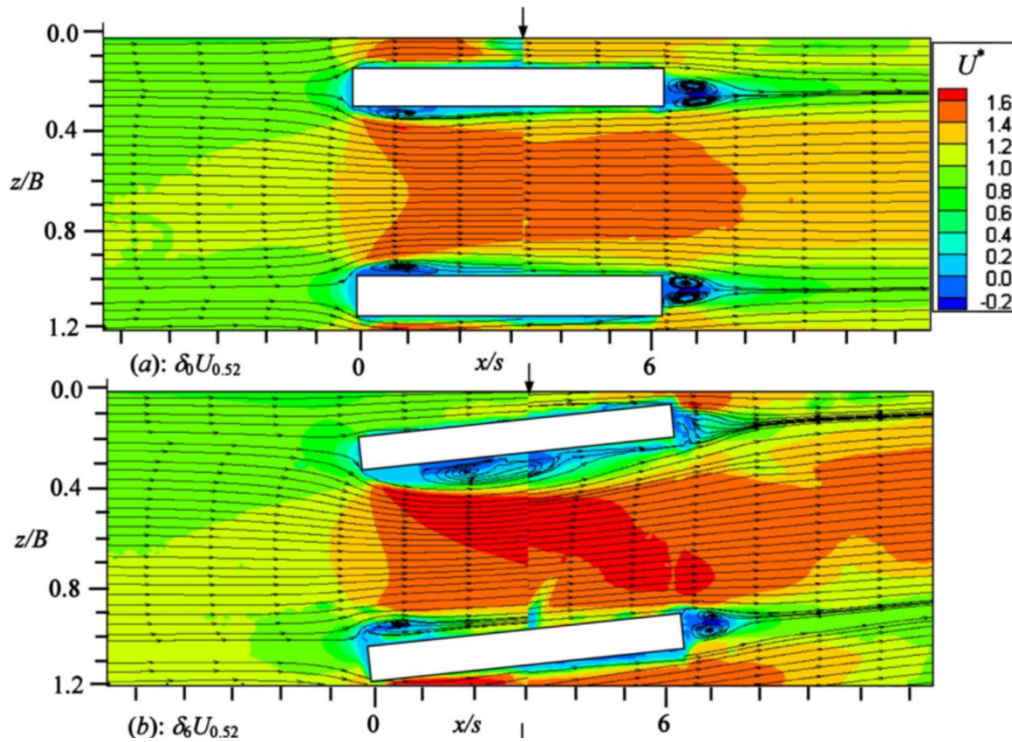


Figure 2.2: Effects of inclined bars on turbulence level and vortex generation (Tsikata et al. (2014), p. 675)

The bar Reynolds number ( $R_b$ ) is important with regards to head loss as it defines the boundary layer around the bar. Eq. 2.1 shows Reynolds number for objects where  $U$  is the approaching velocity,  $b$  is the bar thickness and  $\nu$  is the kinematic viscosity. Drag, or the fluid resistance between the flow and the bars, depends amongst other things on  $R_b$ . The drag coefficient is a parameter that characterizes the drag force associated with a given body shape and  $R_b$ . Therefore, it is important to consider the drag when designing the bar shape. This is especially important in experiments when it comes to the scaling of a model, as too small  $R_b$  values tend to increase the drag coefficient. Seeing as how the drag coefficient is dependent on  $R_b$ , similarity in drag coefficient can only be obtained with similarity in  $R_b$ . A smaller bar scale would create disproportionate values for drag and  $R_b$  in the model compared to the large scale prototype, and subsequently overrate the head loss. Experiments involving trash racks should therefore be carried out with the model as close to a 1:1 scale ratio as possible.

$$R_b = \frac{U \cdot b}{\nu}$$

Eq. 2.1

## 2.2 Head loss calculation

Numerous equations have been proposed to calculate the head losses caused by trash racks. This chapter will however focus on equations applicable for angled trash racks. Eq. 2.3 and Eq. 2.4 are chosen on the background of their inclusion in the Norwegian Water Resources and Energy Directorate's guidelines for intake structures (Jenssen et al., 2006). Additional equations will focus more on recent development in head loss calculation.

The governing parameters for head loss calculation are typically the blockage ratio, defined as total area of bars divided by total rack area, and the flow velocity through the rack. However, the bar shape and bar inclination influence the head losses through a trash rack considerably. The blockage ratio may be calculated in a number of ways based on the angle between the approaching flow and the face of the rack. If the face of the rack is perpendicular to the flow and the bars are aligned with the flow, the calculation of the blockage ratio is fairly easy. However, angled racks with varying bar orientation are not that straight forward. Angled racks with perpendicular bars for example, might appear blocked from the “point of view” of the flow, in which case the redirections of flow caused by the bars has to be accounted for. Eq. 2.2 shows the relationship between the velocity head and the head loss  $\Delta H$ . This relationship is described by the head loss coefficient  $\xi$ .

$$\Delta H = \xi \cdot \frac{U^2}{2g}$$

Eq. 2.2

One of the first to propose an equation for calculating head losses caused by trash racks was Kirschmer (1926). His equation calculated the head losses as a function of bar thickness  $b$ , bar spacing  $e$ , bar shape factor  $k_F$  and the vertical inclination of the rack  $\theta$ . Mosonyi (1966) proposed an extension of Kirschmer’s formula by including an oblique flow factor  $k_\delta$  which takes into account the angle of the approaching flow relative to the rack. The  $k_\delta$  factor is found from tabulated values which depends on the angle of the approaching flow relative to the bars and the blockage number  $b/e$ .

$$\xi_{\text{Kirschmer-Mosonyi}} = k_F \cdot \left(\frac{b}{e}\right)^{\frac{4}{3}} \cdot \sin \theta \cdot k_\delta$$

Eq. 2.3

Meusburger (2002) proposed an equation (Eq. 2.4) that is in many ways similar to the Kirschmer – Mosonyi formula, but goes further in defining the head loss coefficients related to bar shape, blockage ratio and the bars angle relative to the flow. It also includes a multiplicative term  $k_v$  which takes into account the amount of rack area blocked by debris. The factor  $k_F$  is the bar shape factor from Kirschmer (1926),  $\delta$  is the angle between the bars and the flow,  $P$  is the blockage ratio and  $\theta$  is the angle between the racks vertical axis and the velocity vector passing the rack. For vertical racks  $\theta = 90^\circ$ .

$$\xi_{\text{Meusburger}} = k_F \cdot \left(\frac{P}{1-P}\right)^{\frac{3}{2}} \cdot \left(1 - \frac{\delta}{90^\circ}\right) \cdot P^{-1.4 \cdot \tan \delta} \cdot k_v \cdot \sin \alpha$$

Eq. 2.4

Clark et al. (2010) proposed an equation (Eq. 2.5) based on the same parameters as the aforementioned equations. The parameters is the bar shape factor  $\eta$ , the angle  $\delta$  between the flow direction and the bars and the blockage ratio  $P$ .

$$\xi_{\text{Clark}} = 7.43 \cdot \eta \cdot (1 + 2.44 \cdot \tan^2 \delta) \cdot P^2$$

Eq. 2.5

Eq. 2.4 and Eq. 2.5 are based on experiments with similar setups. A plan view of their setups is shown in Figure 2.3, which shows that the downstream flow is aligned with the bars. Eq. 2.4 and Eq. 2.5 have as a consequence reduced applicability for angled racks placed in a straight channel. Especially for racks with bars not parallel with the direction of flow.

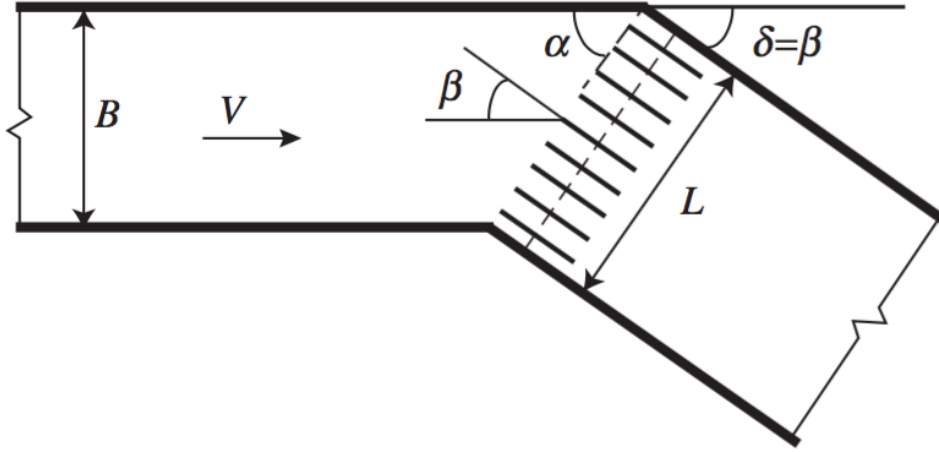


Figure 2.3: Plan view of the experimental setup of Meusburger (2002) and Clark et al. (2010)

Raynal et al. (2013b) also points out that Eq. 2.4 and Eq. 2.5 were both obtained from experiments where the downstream flow was aligned with the bars. They proposed a new equation (Eq. 2.6) to account for cases with angled trash racks in straight channels. Figure 2.4 shows a plan view of the experimental setup.  $k_i$  is the bar shape factor,  $\alpha$  is the angle between the rack and the flow and  $O_g$  is the blockage ratio. Eq. 2.6 is applicable for trash racks inserted in a straight open channel with blocking ratio  $36\% < O_g < 60\%$ , angle between rack and flow  $30^\circ < \alpha < 90^\circ$ , and for rectangular or drop shaped bars with with  $b/p$  ratio close to 0,125. The  $b/p$  ratio is the ratio between bar thickness  $b$  and bar depth  $p$ .

$$\xi_{\text{Raynal(2013b)}} = 1 + k_i \cdot \left( \frac{90^\circ - \alpha}{90^\circ} \right)^{2.35} \cdot \left( \frac{1 - O_g}{O_g} \right)^3 \quad \text{Eq. 2.6}$$

Raynal et al. (2014) argued that angled trash racks with stream wise bars (shown in Figure 2.4 b) have fairly constant head loss coefficients with varying rack angle  $\alpha$ , and suggested that Eq. 2.7 (Raynal, 2013a) might be used. Eq. 2.7 was proposed for predicting head loss through vertical trash racks perpendicular to the channel. The value  $K_i$  in Eq. 2.7 depends on the bar shape, and  $O_g$  is the blockage ratio.

$$\xi_{\text{Raynal(2013a)}} = K_i \cdot \left( \frac{O_g}{1 - O_g} \right)^{1.6} \quad \text{Eq. 2.7}$$

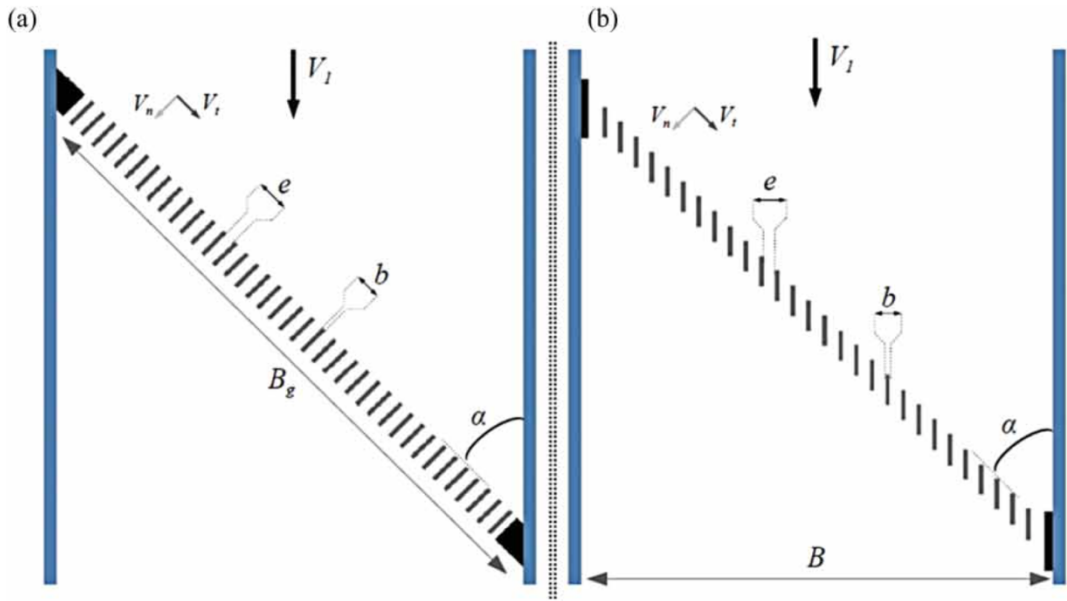


Figure 2.4: Plan view of experimental setup by Raynal et al. (2014)

Eq. 2.8 shows Bernoulli's principle when used for flow in an open channel with a trash rack. The indices  $i$  and  $j$  denotes the water level and mean flow velocity for an upstream and downstream point respectively. The velocities at a given point can be calculated by the Continuity Equation (Eq. 2.9). When the friction head loss  $\Delta H_0$  due to the channel is determined, the head loss  $\Delta H$  caused by the trash rack can be calculated.

$$H_i + \frac{V_i^2}{2g} = H_j + \frac{V_j^2}{2g} + \Delta H + \Delta H_0$$

Eq. 2.8

$$Q = V \cdot A$$

Eq. 2.9

### 2.3 Applicability of the head loss equations

All head loss equations mentioned in the previous chapter has a region of validity based on the experimental setup in their respective studies. Seeing as how each equation is extracted from a limited number of experimental configurations, the equation itself might have limited applicability for cases placed outside the experimental range. Table 2.1 categorizes the equations based on the angle between the rack and the wall of the flume  $\alpha$ , and the ratio between bar spacing  $e$  and bar thickness  $b$ . The  $e/b$  ratio is important due to its link to the blockage ratio, which is the governing parameter for trash rack head loss. The range of  $\alpha$  is especially important for this experiment because angled racks are tested. The bar shape factor values given for each equation also varies considerably. Besides Meusburger (2002), which uses Kirschmer's (1926) bar shape values, the remaining head loss equations employs their own set of values. As a result, it may offer problems in calculating accurate head loss for trash racks with bar shapes that differ from the ones given.

No head loss equations have been proposed for horizontally barred racks insofar it is in any mainstream use. This is probably due to the fact that their use has traditionally been limited for hydropower purposes. Trash racks with horizontal bars typically offer difficulties in cleaning and maintenance compared to racks with vertical bars, as trash and debris can't be removed by simply scraping it off the rack in a vertical motion and out of the water. However, the geometry of the bars is suitable for preventing fish from passing through the bars, given its tall and slim morphology. Although there are no equations specifically for trash racks with horizontal bars, it is reasonable to assume that it is governed by the same parameters as vertically barred racks. For that reason, the given equations might be applicable to horizontally barred racks.

Table 2.1: Comparison of max. and min. values of  $\alpha$  and  $e/b$  in different studies

Equation	$\alpha$		$e/b$	
	Min	Max	Min	Max
Kirschmer –Mosonyi (1966)	30	90	1	5
Meusburger (2002)	60	90	1	9
Clark et al. (2010)	60	90	1.75	11.6
Raynal et al. (2013b)	30	90	1	3
Raynal et al. (2013a)	90	90	1	3

## 2.4 Difficulties regarding trash racks and downstream migration of fish

Hydropower structures are obstacles that hinder downstream migration of European silver eel and smolts. In the downstream migration fish are often injured or killed when trying to pass these obstacles, either by impingement on trash racks or by passing through turbines. Since the early 1980s and almost continent wide decline of 90 % is observed for European silver eel in European water courses (Dekker, 2003). In an attempt to counter this trend in Europe the EU Eels Regulation (EC, 2007) requires member states to aim for 40 % escapement of eel biomass to the sea, in relation to anthropogenic mortalities. As a consequence, there is an increased focus on trash racks being fish-friendly.

To ensure that smolts and eels do not pass through the trash rack or come in contact with the trash rack at all, certain boundary conditions has to be set. Bar spacing should not be wider than the width of the approaching fish. However, research in smolt behaviour shows that trash racks were found to have a repelling effect on the smolts when the bar spacing was less than 40 mm (Larinier and Travade, 2002). For trash racks to be characterized as fish-friendly the bar spacing should be less than 25 mm for smolts and 20 mm for silver eels, and the trash racks should be inclined to or angled to guide the fish towards a bypass (Courret and Larinier, 2008). Water velocities towards the trash rack should also not exceed the cruising speed of a given species. Many different boundary velocities have been proposed, but a recurring number is 0.5 m/s (Larinier and Travade, 2002).

To guide the fish safely past the trash racks bypasses have to be implemented. However, bypasses have to be designed to accommodate the behaviour of smolts and silver eels. The acceleration to the entrance of the bypass should not be too high seeing as how fish are sensitive to steep velocity gradients. The flow in the bypass should also be sufficiently high enough related to the turbine discharge. Experiments in France show that bypass discharges between 2% and 10% of the turbine discharge is satisfactory, with low numbers acceptable if there is an inclined guiding structure (Larinier and Travade, 2002).

## 3 Methodology

### 3.1 Experimental setup

#### 3.1.1 Flume and boundary conditions

The flume used in this experiment was a 12.5 m long, 1 m wide and 1 m deep experimental flume from Armfield Ltd, shown in Figure 3.1. The flume operates with two circulating pumps with a combined capacity of 450 l/s, which can be adjusted by a set of valves. The slope of the flume can also be adjusted, but will remain horizontal throughout this experiment. The bottom of the flume is made up of aluminium plates, making a smooth surface and reducing the effects of friction. The initial water level will be kept at 0.5 m throughout the experiment.



Figure 3.1: Armfield Ltd flume used in this experiment

#### 3.1.2 Trash racks and bypass

Six different types of acrylic trash rack models were designed for and tested in this experiment. Each rack is 660 mm tall ( $H_r$ ) and 1810 mm wide ( $B_r$ ), but with different types of bars and bar arrangements. To avoid scaling issues related to drag and  $R_b$ , the trash racks models have a 1:1 scale. All six racks have the same angle relative to the wall of the flume  $\alpha = 30^\circ$ , and all racks are vertical  $\theta = 90^\circ$ . A plan view of the trash rack setup is shown in Figure 3.2 and Figure 3.4.

At the centre of the flume acrylic plates are placed on the bottom to fit the trash racks. A slot is made from the entrance of the bypass across the flume to the opposite wall, in which the trash racks are easily fitted. The bypass is located on the right hand side relative to the direction of the flow, and is 95 mm wide. At the entrance of the bypass a  $30^\circ$  ramp is placed and extends up to 350 mm above the flume bed. The reason for placing a ramp at a bypass entrance is to accelerate the flow to lead the fish towards the bypass, and to guide the bottom dwelling eels up and into the bypass. A 668 mm tall wall separates the bypass and the main channel downstream of the rack, extending to the end of the flume. The bypass can be seen in plan view in Figure 3.2 and and Figure 3.4, and in side view in Figure 3.3. The centre of the trash racks is placed 5.44 meters from the end of the flume.

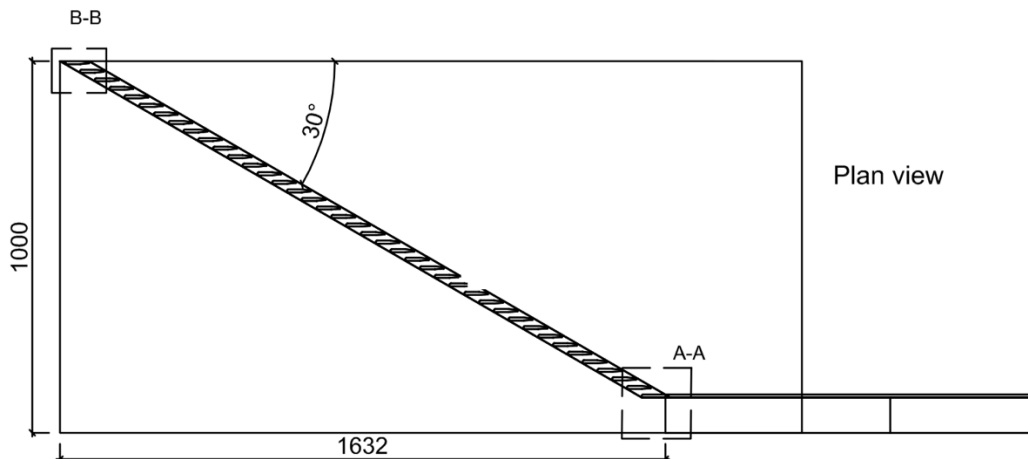


Figure 3.2: Plan view of the rack and the bypass (Rack II)  
(Fig. made by Szabo-Meszaros, Marcell)

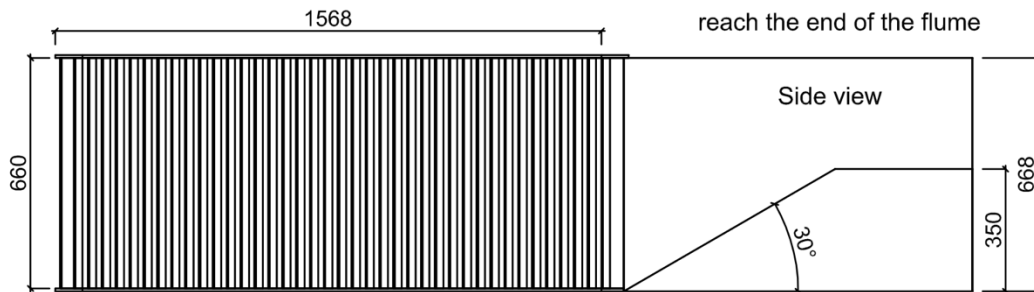


Figure 3.3: Side view of the rack and by pass (Fig. made by Szabo-Meszaros, Marcell)

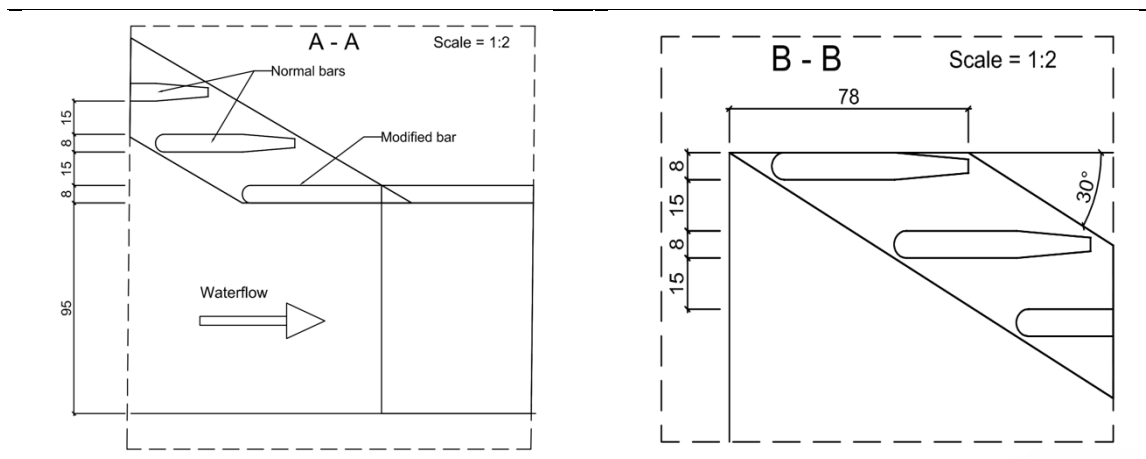


Figure 3.4: Plan view of sections of the rack and bypass (Rack II)  
(Fig. made by Szabo-Meszaros, Marcell)

The six mentioned bar configurations are shown in Figure 3.2 and Table 2.1. The different bar configurations consist of three different sets of bar arrangement, each with rectangular and drop shaped bars. The number of bars  $n$  in each rack varies due to the angle and arrangement of the bars. All bars in rack I-VI have 15 mm spacing between them and are 8 mm wide and 64 mm deep, which classifies the bars as long. The narrow spacing of 15 mm is due to the criteria set for

fish-friendly trash racks. The length of the bars depends on whether the bars are vertical or horizontal. Vertical bars are 660 mm and horizontal bars are 1810 mm long. The blockage ratio is calculated as total area occupied by the bars divided by total rack area, where the width of the rack is set to the axis perpendicular to the bar orientation. For Rack I-II and V-VI the rack width is set to  $B = 0.905$  m and for Rack III-IV it is set to  $B_r = 1.81$  m. Rack V-VI have four streamwise vertical support bars with identical dimensions as the remaining bars, which is accounted for in the blockage ratio. Both types of bar shapes are shown in fig. 3.3. The design of the racks and bars is based on the work of Raynal et al. (2013a, 2013b).

Table 3.1: Description of trash racks

Rack	Description	Bar shape	n	Og
I	Bars parallel with the flow	Rectangular	40	0.354
II	Bars parallel with the flow	Drop shaped	40	0.354
III	Bars perpendicular to the axis of the rack	Rectangular	76	0.336
IV	Bars perpendicular to the axis of the rack	Drop shaped	77	0.340
V	Horizontal bars	Rectangular	28	0.363
VI	Horizontal bars	Drop shaped	28	0.363

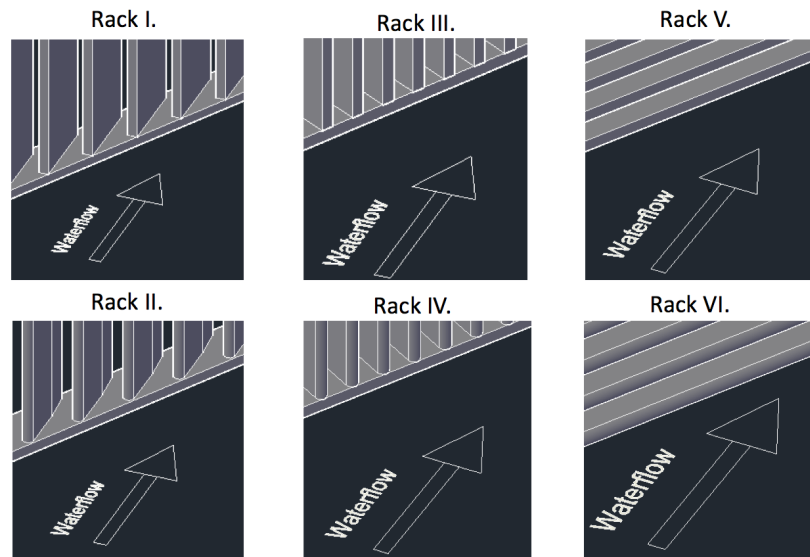


Figure 3.5: Front view of rack I-VI (Fig. made by Szabo-Meszaros, Marcell)

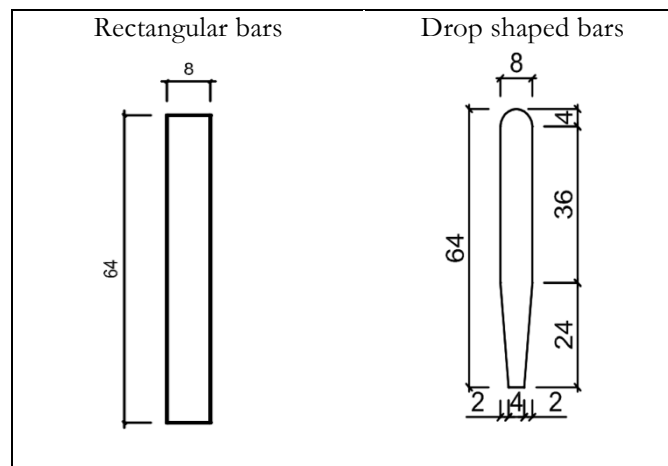


Figure 3.6: Bar shapes with values in mm (Fig. made by Szabo-Meszaros, Marcell)

### 3.1.3 Head loss measurements

The head loss measurements are done with piezometers. The flume has several small valves integrated throughout its length. Pressure tubes are attached to the valves and to four open cylinders. The water level is then measured by a Digimatic Height Gage by Mitutoyo (0.01 mm resolution) in each cylinder, and recorded. Three piezometers are placed upstream of the rack and one downstream. The piezometer layout is shown in Figure 3.7. Table 3.2 shows the positioning of the piezometers and the rack along the length of the flume.  $H_4$  is the piezometer furthest downstream. The distances are relative to the downstream end of the flume.

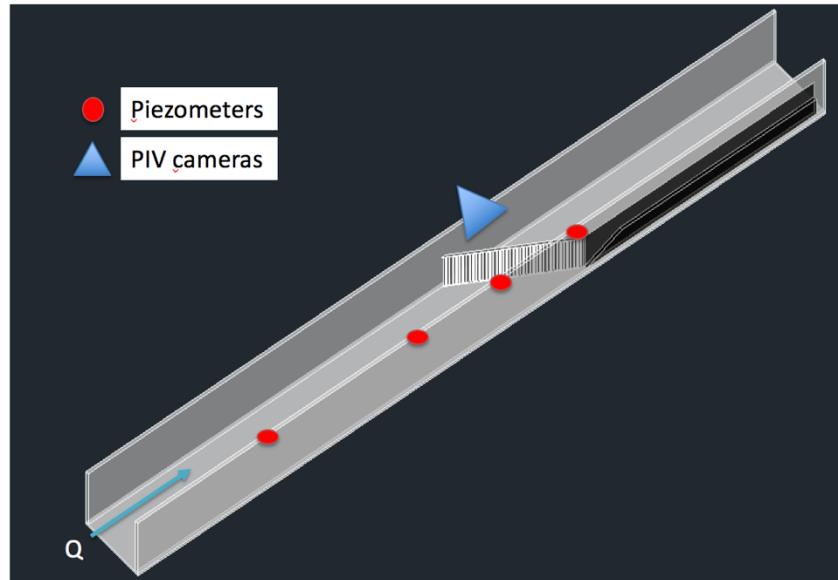


Figure 3.7: Piezometer layout (Fig. made by Szabo-Meszaros, Marcell)

Table 3.2: Piezometer layout. Distance is from the inlet.

Piezometer/rack	$H_1$	$H_2$	$H_3$	Rack	$H_4$
Position [m]	3.125	5.625	6.875	7.06	8.125

### 3.1.4 Particle Image Velocimetry

Quantitative flow field measurements near the trash racks will be carried out with the Volumetric 3-component Velocimetry (V3V PIV) system from TSI Inc. The V3V system is a novel PIV system which has the ability to measure 3-component 3-dimensional vector data in a  $140 \times 140 \times 100 \text{ mm}^3$  cuboid volume. This makes it possible to map a 3D velocity profile near the racks. The flow is seeded with  $55 \mu\text{m}$  polyamide particles. The measurement volume is illuminated by a Litron Nd:YAG Nano L PIV laser ( $\lambda = 532 \text{ nm}$ ), emitting a laser cone after passing through a TSI LaserPulse Light Arm. Images are acquired by three Powerview CCD model 4MP-180 cameras, mounted in a triangular fashion on a V3V 9000 CS camera mount. All hardware is connected to and controlled by the Insight V3V 4G software by TSI.

The V3V system measures the displacement of seeding particles over a known amount of time to determine the local velocity. The seeding particles flows through a measurement volume, where a cone of laser light illuminates the particles. Two short pulses of laser light are then fired, separated by an adjustable time interval. The three cameras will each take a picture at the laser pulses. A particle inside the control volume will then be captured from three different angles, forming a triangle. By measuring the size of the triangle, or “triplet”, relative to a focal plane, the depth position of the particle can be found. An illustration of this principle is shown in Figure

3.8. The centre of the triangle is the x and y position of the particle. This means that the three-aperture camera probe can determine 3D positions of the particles at each laser pulse (Pothos et al., 2009).

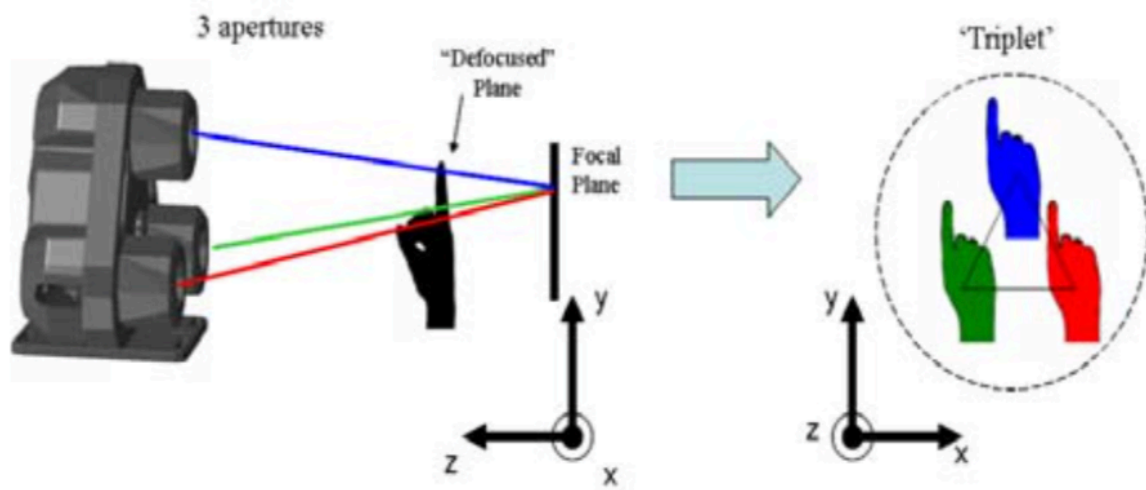


Figure 3.8: Concept of a "Triplet" in V3V (Pothos et al. 2009, p. 27)

The images from the V3V camera probe is then imported into the INSIGHT V3V 4G software. The software scans the images for triangle patterns to determine the particles 3D positions. Advanced particle tracking algorithms is then applied to determine a particles displacement, now seen as pixels with varying light intensity, between each frame obtaining true 3 component velocity data. Further information on the V3V used is closer described in “Near bed flow field over permeable and impermeable beds” (Øvregård, 2015).

For rack I-II and rack V-VI The V3V system were placed to measure at the centre, and just downstream, of the rack. The light arm is mounted above the water surface, illuminating the measurement volume from above. To ensure uniform lighting of the measurement volume, a moveable acrylic box (Figure 3.9) was mounted on the rack. The bottom of the box was placed to just breach the water surface with the laser placed right above. This was done to remove the effects of moving water surface distorting the light from the laser. Another measure to increase illumination of the measurement volume was to place a mirror at the bottom of the flume. The centre of each rack was painted black to reduce background noise due to reflection of the laser light.

For rack III and IV the V3V system could not be used. Due to the orientation of the bars, the flow was directed towards the cameras and the measurements revealed that the V3V system has problems identifying seeding particles when the main flow is not perpendicular to the view of the cameras. Instead, a 2D PIV system was set up by using a single camera capturing images directly above the measurement area, and by emitting a single horizontal laser sheet from the side of the flume. The laser sheet was placed at the middle of the water depth, approximately at the centre of the 3D measurement volume.

After acquiring the downstream data for the racks, the V3V system was set up on the opposite side of the flume to acquire upstream data. By doing this, upstream flow characteristics can be obtained and examined to evaluate the fish friendliness. This is especially related to the 0.5 m/s

velocity boundary condition. Data capturing upstream was done with the V3V system for all racks, seeing as how the flow is perpendicular to camera view.

V3V system captured pictures at a laser frequency of 15 Hz over 200 seconds, yielding 3000 single captures. With three cameras capturing twice at each laser pulse, and each frame being approximately 4 MB, the total amount of data expected from one rack at a given discharge is roughly 72 GB.

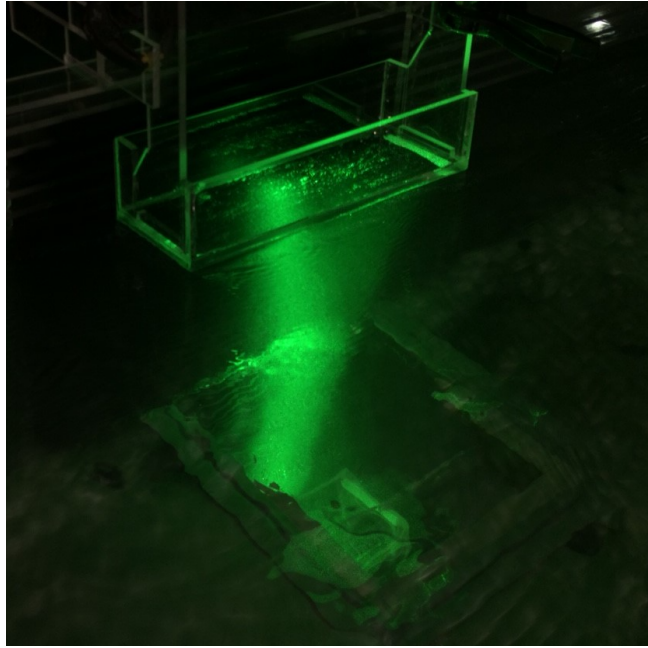


Figure 3.9: The measurement area just downstream of the rack  
(Picture taken by Szabo-Meszáros, Marcell)

### 3.2 Experimental procedure

Each rack was tested under six different discharges, from 50 l/s to 200 l/s with a 30 l/s step. This gave a total of 36 different experimental configurations to carry out. However, the V3V system was only applied to the 200 l/s and 170 l/s discharges, while the head loss measurements are done for all 36 configurations. The reason for the limited use of the V3V system is to save time, and to focus on the two highest discharges which gives approaching flow velocities close to the boundary condition of 0.5 m/s previously mentioned.

Upon placing a rack in the flume, the pumps were turned on. When the flow reached equilibrium and proper measures were carried out to obtain satisfactory particle detection, the V3V system was set to capture. Figure 3.10 shows the experiment area, looking upstream from the downstream side of the rack, during a V3V capture. After the image capturing was done, the water depths were measured by the piezometers and recorded, and subsequently used to determine the head loss. The discharge was then adjusted and the process repeated, but without the V3V system capturing images for discharges below 170 l/s. The water level readings were done three times for each piezometer, and after a change in discharge the flow was allowed to settle for 10 minutes. This was done to remove some uncertainty connected to the measurement of the water levels

To ensure that the particle detection yield was sufficient for each experiment configuration test captures were conducted. This was done by capturing a small number of images, and running the particle detection sequence in the V3V system's software Insight V3V 4G. If the particle detection yield was insufficient changes were made, and a new test captures were carried out. This included adjusting the seeding particle amount, adjusting the parameters in the software and/or redo the calibration. Water quality issues also occurred. Dirt and unwanted particles interfering with the particle detection was at times a problem. This is probably due to the accumulation of old seeding particles and dirt in the circulation pumps. The flume collects water from a large laboratory basin, which over time will accumulate dirt from previous experiments. As a result, the flume occasionally had to be filled up with tap water, which was a lengthy affair. The post – processing of the data from each capture also require a lot of time given the amount of data collected. Post-processing for one rack at a certain discharge usually takes 4-5 days. As a consequence, the time needed for acquiring satisfying data from one rack at a given discharge is roughly a week's time.

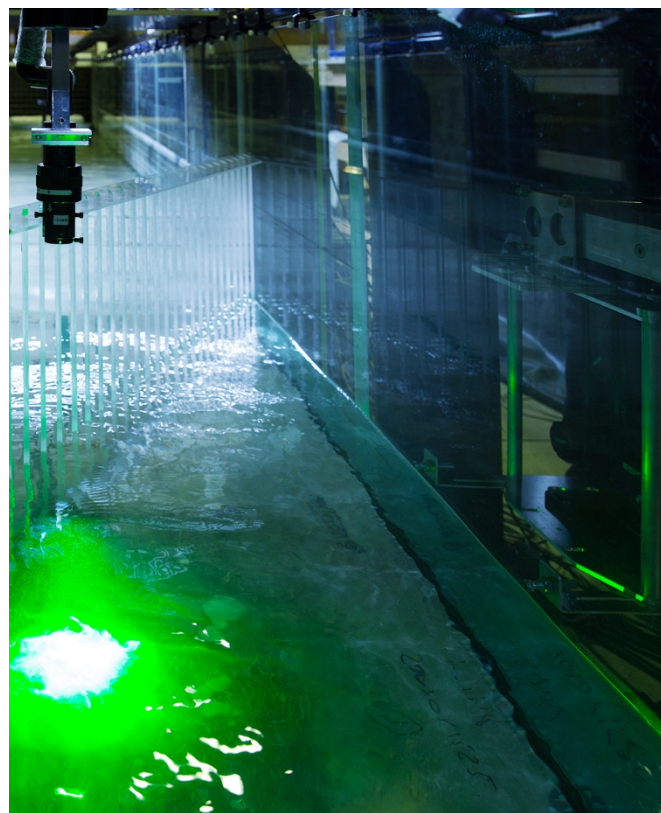


Figure 3.10: Picture of the rack, laser (top left) and V3V camera probe (middle right)  
(Picture taken by Navaratnam, Christy Ushanth)

Head loss measurements without the racks were done for every discharge to estimate the energy loss due to friction in the flume ( $\Delta H_0$ ).  $\Delta H_0$  was measured between piezometer 2 and 4. In addition, velocity and water depth measurements were carried out in the bypass just past the ramp to calculate the amount of discharge passing through it. This was however only done for  $Q = 200$  l/s and  $Q = 170$  l/s due to time restrictions. The velocity measurements were carried out with a Nortek Vectrino + Acoustic Doppler Velocimeter. The measurements were carried out at four points downstream of the end of the ramp, and then averaged. Two vertical points 90 mm, and two points 190 mm, downstream of the end of the ramp. The vertical points were 42 and 45 mm above the floor of the bypass, making the four points form a rectangle. The water depths were obtained by reading of a measuring tape attached to the wall of the flume.

## 4 Results

### 4.1 Head loss and head loss coefficients

The water level measurements from the piezometer readings are shown in Figure 4.1. It shows the relative water surface for each rack at the different discharges tested. The direction of flow is from right to left. Figure 4.1 only shows the relative elevation head directly measured. It does not take into account head loss due to friction, different velocity heads or the different cross sectional area upstream and downstream of the rack. The values used for making the plots in Figure 4.1 can be seen in Appendix B.

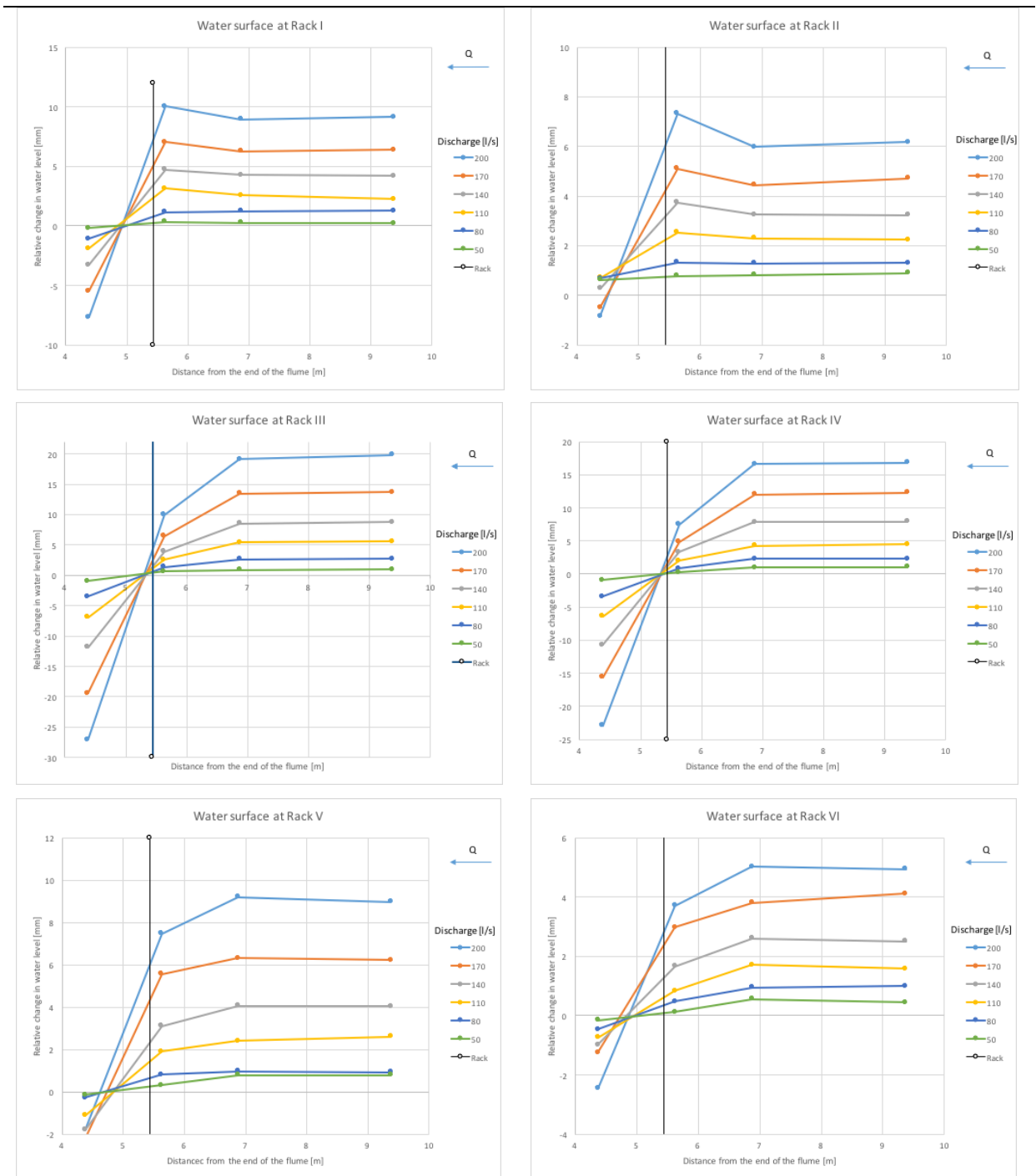


Figure 4.1: Water surface visualisation for Rack I-VI.

The water level values from piezometer 2 and 4 are chosen to calculate the head loss  $\Delta H$ , by using Eq. 2.8.  $H_4$  and  $V_4$  are the water level and velocity at piezometer 4, while  $H_2$  and  $V_2$  denotes the water level and velocity at piezometer 2. The piezometer layout is shown in fig. 3.7 and table 3.2.  $\Delta H_0$  is the measured head loss due to friction, and is shown in Table 4.1 for different discharges. This makes it possible to calculate the head loss  $\Delta H$  through the trash rack by using Eq. 2.2. However, to use Eq. 2.2 properly it is important to apply the velocity defined for each head loss equation in order to compare the measured results with them. The equations proposed by Kirschmer-Mosonyi (1966), Meusburger (2002) and Clark et al. (2014) all define the velocity as the discharge passing through the rack divided by the submerged area of the rack. This is opposed to Raynal et al.'s equations who uses the mean velocity of the channel 1 m upstream of the rack. For Raynal et al.'s equations  $V_2$  will be used as it is 1.4 meter upstream and closest to the criterion. For the remaining equations the mean velocity  $V_3$  right in front of the rack is used. It is important to notice that the cross sectional area downstream of the rack is reduced due to the width of the bypass. The discharge passing through the trash rack is also reduced by the amount of water passing through the bypass. This is taken into account when calculating  $V_3$  and  $V_4$ . For  $V_3$  the discharge passing through the rack is calculated as total discharge minus the discharge passing through the bypass, and the width of the rack is set to  $B = 0.905$  for all racks. For  $V_4$  the discharge passing through the bypass is also subtracted, and the width of the channel is reduced to 0.905 m. The bypass discharge for each total discharge and rack is shown in Table 4.2, based on measured values given in Appendix B. The velocities used for calculating and predicting head losses are shown in Table 4.3. As mentioned in chapter 3.2 the discharge measurements in the bypass was only carried out for  $Q = 170$  l/s and  $Q = 200$  l/s. For the remaining total discharges, the values were extrapolated. The calculated head losses for all racks and discharges are given in Table 4.4.

Table 4.1: Friction head loss  $\Delta H_0$  between  $H_2$  and  $H_4$  at different discharges

<b>Q [l/s]</b>	<b><math>\Delta H_0</math> [mm]</b>
<b>200</b>	3.1
<b>170</b>	2.2
<b>140</b>	1.6
<b>110</b>	0.9
<b>80</b>	0.7
<b>50</b>	0.1

Table 4.2: Discharge through the bypass for each rack at a given total discharge.

All values are in l/s.

<b>Q [l/s]</b>	<b>Rack I</b>	<b>Rack II</b>	<b>Rack III</b>	<b>Rack IV</b>	<b>Rack V</b>	<b>Rack VI</b>
200	7.50	6.38	10.03	10.43	6.35	5.78
170	6.41	5.43	9.04	8.74	5.21	4.93
140	5.31	4.47	8.05	7.05	4.07	3.79
110	4.22	3.52	7.06	5.36	2.93	2.65
80	3.12	2.57	6.07	3.67	1.80	1.52
50	2.03	1.62	5.08	1.98	0.66	0.38

Table 4.3: Velocity data sorted by rack and discharge

Q [l/s]	Rack I	Rack II	Rack III	Rack IV	Rack V	Rack VI
<b>V<sub>2</sub> [m/s]</b>						
200	0.393	0.395	0.385	0.387	0.393	0.396
170	0.336	0.337	0.331	0.332	0.336	0.337
140	0.278	0.278	0.275	0.276	0.278	0.279
110	0.219	0.219	0.218	0.218	0.219	0.219
80	0.160	0.160	0.159	0.159	0.160	0.160
50	0.100	0.100	0.100	0.100	0.100	0.100
<b>V<sub>4</sub> [m/s]</b>						
200	0.432	0.429	0.444	0.439	0.430	0.431
170	0.366	0.364	0.370	0.368	0.366	0.366
140	0.300	0.299	0.299	0.300	0.301	0.302
110	0.235	0.235	0.231	0.234	0.237	0.238
80	0.170	0.171	0.165	0.170	0.173	0.174
50	0.106	0.107	0.099	0.106	0.109	0.110
<b>V<sub>3</sub> [m/s]</b>						
200	0.417	0.422	0.412	0.413	0.422	0.426
170	0.357	0.360	0.351	0.353	0.360	0.363
140	0.295	0.297	0.289	0.292	0.299	0.300
110	0.232	0.234	0.226	0.115	0.236	0.237
80	0.170	0.171	0.163	0.168	0.173	0.173
50	0.106	0.106	0.099	0.106	0.109	0.110

Table 4.4: Calculated head loss  $\Delta H$  [mm] from measured data

Q [l/s]	Rack I	Rack II	Rack III	Rack IV	Rack V	Rack VI
200	11.8	2.3	40.6	34.2	6.4	2.9
170	8.4	1.7	29.2	24.1	5.2	1.8
140	5.3	0.8	18.1	16.2	3.6	1.3
110	3.2	0.3	11.2	9.4	2.2	1.1
80	1.5	-0.3	5.4	4.8	0.3	0.5
50	0.3	0.02	1.8	1.8	0.7	0.5

Chapter 2.2 describes that the experimental setup for obtaining the given head loss equations are quite dissimilar. Table 2.1 shows the region in which the given head loss equations are applicable. It shows that the head loss equations can not be universally applied to the racks used in this experiment. The racks'  $e/b$  ratio is 1.875, which satisfies requirements for all mentioned head loss equations. However, all racks have the same angle  $\alpha$  between the rack and the flume wall. This limits the applicability of Meusburger's (2002) and Clark et al.'s (2010) equations. Raynal et al. (2014) argues that the head loss coefficient of angled trash racks with stream wise bars can be calculated by using any head loss equation for vertical and non-angled racks, due to the negligible impact of the racks angle on head losses. This suggests that the aforementioned head loss equations can be applied to Rack I-II. None of the given head loss equations include experiments including horizontally barred racks. It is however governed by the same parameters, so the given equations might yield approximate results. Seeing as how the angle of racks with horizontal bars arguably won't redirect the flow through the rack, it is reasonable to assume that the given equations can be applied to Rack V-VI in the same manner as Rack I-II.

#### 4.1.1 Kirschmer-Mosonyi (1966)

Eq. 2.3. The  $b/e$  ratio is used to account for the blocking in Kirschmer-Mosonyi's equation, not the blockage ratio used in the remaining equations. As a consequence,  $b/e = 0.533$  is the same for all racks. The shape factor  $k_F$  for rectangular bars is set to 2.42. The drop shaped bars utilized in this experiment does not correspond with the bar shapes given by Kirschmer-Mosonyi. The bar shape closest to the ones used in this experiment was chosen. The values are obtained from Jenssen et al. (2006), and the bars used are K and D for rectangular and drops shaped bars respectively. For the drop shaped bars  $k_F$  was set to 1.04. The inclination, denoted by  $\theta$ , is  $90^\circ$  for all racks. The oblique flow factor  $k\delta$  is found from tabulated values in Jenssen et al. (2006). The oblique flow angle  $\delta$  is assumed to  $0^\circ$  for rack I-II and rack V-VI, given that the flow is approaching the bars head on. For rack III-IV the angle between the orientation of the bars and the oncoming flow is  $60^\circ$ . The calculated  $\xi$  values for each rack are given in Table 4.5.

Table 4.5: Kirschmer-Mosonyi - calculated head loss coefficients

Parameter	Rack I	Rack II	Rack III	Rack IV	Rack V	Rack VI
$k_F$	2.42	1.04	2.42	1.04	2.42	1.04
$b/e$	0.533	0.533	0.533	0.533	0.533	0.533
$\theta$	90	90	90	90	90	90
$k\delta$	1	1	3.7	3.7	1	1
$\xi_{\text{Kirschmer-Mosonyi}}$	1.05	0.45	3.87	1.66	1.05	0.45

#### 4.1.2 Meusburger (2002)

Eq. 2.4 shows how to calculate the head loss coefficient proposed by Meusburger (2002). The bar shape factor  $k_F$  is the same as for the equation proposed by Kirschmer – Mosonyi (1966). The blockage ratio  $P$  is calculated according to the definition given in Chapter 2. The oblique flow angle  $\delta$  is assumed to be  $0^\circ$  for rack I-II and rack V-VI and  $60^\circ$  for rack III-IV. The  $k_V$  value does not apply in this experiment due to the absence of blocking debris and is set to 1. The calculated  $\xi$  values for each rack are given in Table 4.6.

Table 4.6: Meusburger - calculated head loss coefficients

Parameter	Rack I	Rack II	Rack III	Rack IV	Rack V	Rack VI
$k_F$	2.42	1.04	2.42	1.04	2.42	1.04
$P$	0.354	0.354	0.336	0.340	0.363	0.363
$\delta$	$0^\circ$	$0^\circ$	$60^\circ$	$60^\circ$	$0^\circ$	$0^\circ$
$\theta$	$90^\circ$	$90^\circ$	$90^\circ$	$90^\circ$	$90^\circ$	$90^\circ$
$k_V$	1	1	1	1	1	1
$\xi_{\text{Meusburger}}$	0.98	0.42	4.09	1.75	1.04	0.45

#### 4.1.3 Clark et al. (2010)

Based on Eq. 2.5 proposed by Clark et al. (2010) the head loss coefficients can be calculated. The blockage ratio  $p$  is the same as for the other equations. The bar shape factor  $\eta$  is taken from Clark et al.'s (2010) own values. For the rectangular bars  $\eta = 1$ . None of the bars used in Clark et al. (2010) are identical to the drop shaped bars in this experiment. Therefore, the closest looking bar shape was chosen, which was bar S3-T2. The oblique flow angle  $\delta$  is assumed to be  $0^\circ$  for Rack I-II and Rack V-VI, and  $60^\circ$  for Rack III-IV. The calculated  $\xi$  values for each rack are given in Table 4.7.

Table 4.7: Clark et al. (2010) - calculated head loss coefficients

Parameter	Rack I	Rack II	Rack III	Rack IV	Rack V	Rack VI
$\eta$	1	0.147	1	0.147	1	0.147
$\delta$	0°	0°	60°	60°	0°	0°
$P$	0.354	0.354	0.336	0.340	0.363	0.363
$\xi_{\text{Clark}}$	0.93	0.14	1.52	0.23	0.98	0.14

#### 4.1.4 Raynal et al. (2013b)

Eq. 2.6 are determined by the blockage ratio  $O_g$ , the angle of the rack  $\alpha$  and the bar shape factor  $k_i$ . The bars shape factor for rectangular bars is  $k_{pr} = 1.69$  and  $k_{ph} = 2.78$  for drop shaped bars. As this equation is obtained from experiments with angled racks  $\alpha$  is set to 30° for all racks. The calculated  $\xi$  values for each rack are given in Table 4.8.

Table 4.8: Raynal et al. (2013b) - calculated head loss coefficients

Parameter	Rack I	Rack II	Rack III	Rack IV	Rack V	Rack VI
$k_i$	1.69	2.78	1.69	2.78	1.69	2.78
$O_g$	0.354	0.354	0.336	0.340	0.363	0.363
$\alpha$	30°	30°	30°	30°	30°	30°
$\xi_{\text{Raynal (2013b)}}$	4.98	7.55	6.04	8.81	5.12	7.77

#### 4.1.5 Raynal et al. (2013a)

Eq. 2.7 are only dependent on the blockage ratio  $O_g$  and the bar shape factor  $K_i$ . This is because the equation is proposed for vertical and non-angled racks. The bars shape factor for rectangular bars is  $K_{pr} = 2.89$  and  $K_{ph} = 1.7$  for drop shaped bars. The calculation of  $O_g$  is the same as for Eq. 2.6 by Raynal et al.(2013b). The calculated head loss coefficients for each rack are presented in Table 4.9.

Table 4.9: Raynal et al. (2013a) - calculated head loss coefficients

Parameter	Rack I	Rack II	Rack III	Rack IV	Rack V	Rack VI
$K_i$	2.89	1.7	2.89	1.7	2.89	1.7
$O_g$	0.354	0.354	0.354	0.340	0.363	0.363
$\xi_{\text{Raynal (2013a)}}$	1.10	0.65	0.97	0.59	1.17	0.69

Table 4.10 compares the calculated head loss coefficients from the equations and the experimental data. Table 4.10 show all calculated values regardless of applicability of the given equations.

Table 4.10: Predicted head loss coefficients  $\xi$ 

Equations	Rack I	Rack II	Rack III	Rack IV	Rack V	Rack VI
Kirschmer-Mosonyi (1966)	1.05	0.45	3.87	1.66	1.05	0.45
Meusburger (2002)	0.98	0.42	4.09	1.66	1.04	0.25
Clark et al. (2010)	0.93	0.19	1.52	0.31	0.98	0.20
<b>Measured <math>\xi</math> (<math>V_3</math>)</b>	<b>1.30</b>	<b>0.26</b>	<b>2.13</b>	<b>1.71</b>	<b>0.75</b>	<b>0.29</b>
Raynal et al. (2013a)	1.10	0.65	0.97	0.59	1.17	0.69
Raynal et. al (2013b)	4.98	7.55	6.04	8.81	5.12	7.77
<b>Measured <math>\xi</math> (<math>V_2</math>)</b>	<b>1.48</b>	<b>0.29</b>	<b>5.30</b>	<b>4.39</b>	<b>0.86</b>	<b>0.34</b>

Figure 4.2 shows the measured head loss  $\Delta H$  for all racks and discharges plotted together. The values are obtained from Table 4.4. The plot comparing the predicted and measured is given in Figure 4.3. Eq. 2.2 is used for calculating the predicted head losses based on the values of Table 4.3 and Table 4.10, and compared to the measured head losses from Table 4.4. Comparison of predicted and measured head loss will only be presented for  $Q = 170 \text{ l/s}$  in this chapter, but additional plots for the remaining discharges are placed in Appendix B.

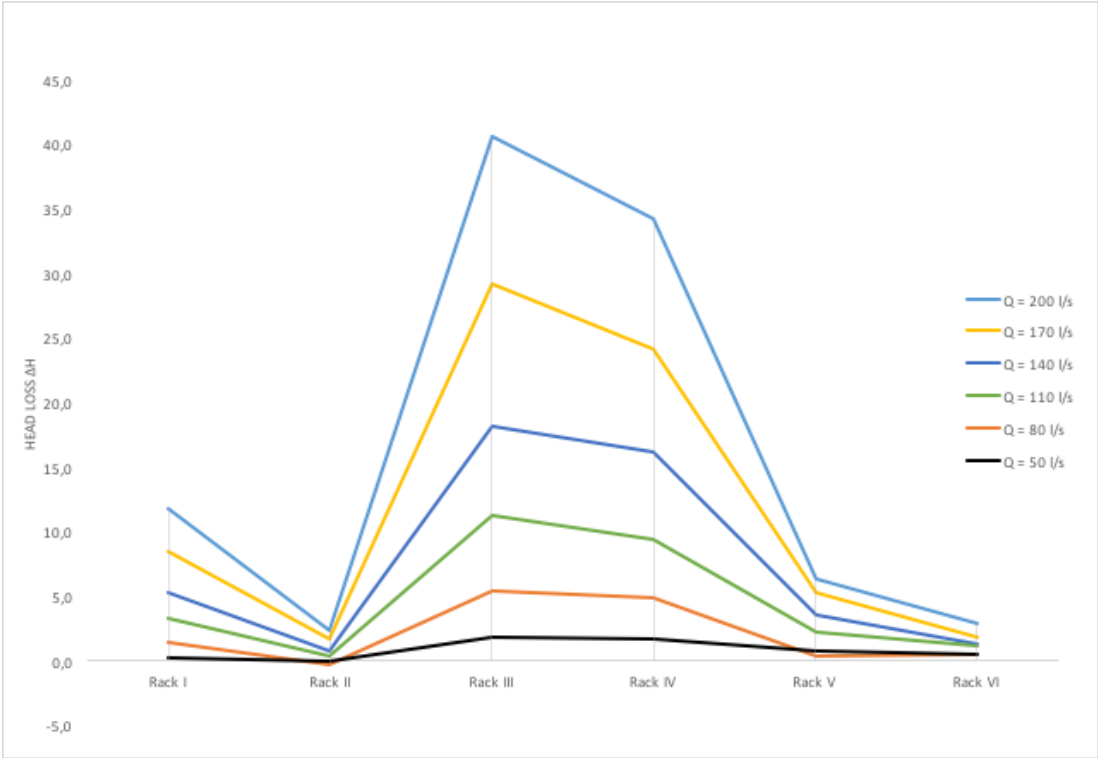


Figure 4.2: Measured head losses for all racks and discharges

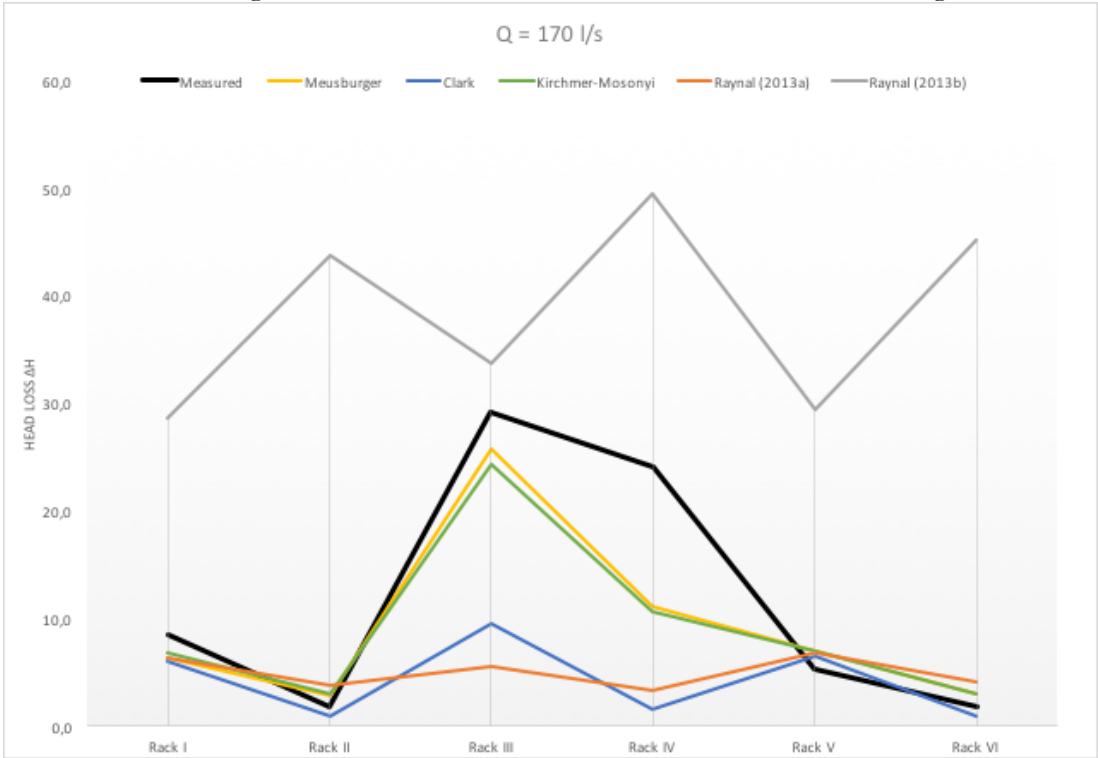


Figure 4.3: Comparison of predicted and measured head loss  $\Delta h$  at  $Q = 170 \text{ l/s}$

## 4.2 V3V results

After the post-processing of the V3V captures is done a large CSV file is extracted. The file contains spatial and time averaged 3 component velocities and velocity fluctuations for 2 mm x 2 mm cells throughout the volume. This data can be used in any numerical computing software, like MATLAB or Microsoft Excel. The INSIGHT V3V 4G software has a built in function which plots the measured data. The plots presented in this sub chapter are all obtained from the INSIGHT V3V 4G software, and made by Christy Ushanth Navaratnam.

Figure 4.4 and Figure 4.5 shows examples of isometric velocity plots created by INSIGHT V3V 4G. The x – axis is parallel with the flow. The V3V system defines the centre of the x-axis as the middle of the flume with values increasing from left to right. This means that velocities parallel with the flow will have different signs depending on which side the measurements is obtained from. This has to be accounted for. In the case for the downstream measurements in this experiment the V3V system is placed on the left hand side of the flume due to the geometry of the trash rack. The y-axis denotes the vertical distance over floor of the flume, while the z- axis denotes the length from the cameras ( $z = 0$ ). The y and z-axis act the same for downstream and upstream measurements. Note that the distance from the cameras increase with negative numbers, i.e.  $z = -720$  is closer to the cameras than  $z = -800$ . Figure 4.6 shows an example of a top view of a certain slice along the y-axis of a measurement volume like the one in Figure 4.4. Figure 4.7 shows an example of a side view of a certain slice along the z-axis of a measurement volume like the one in Figure 4.5. The bars showed in Figure 4.4, Figure 4.5, Figure 4.6 and Figure 4.7 serves to illustrate the rack placement and different bar configurations relative to the measurement volume. They do not show the exact position of the bars, correct bar size and shape or true bar inclination. The velocity magnitude plots in this chapter are presented in m/s.

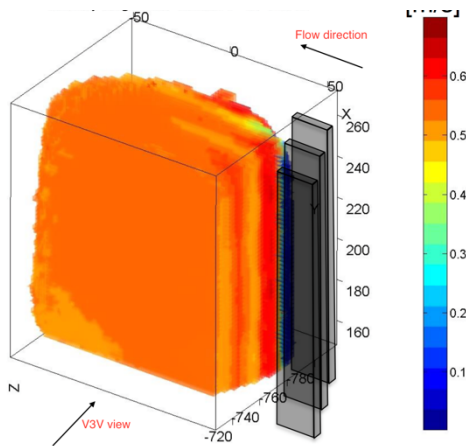


Figure 4.4: Example of V3V isometric velocity plot with vertical bar placement

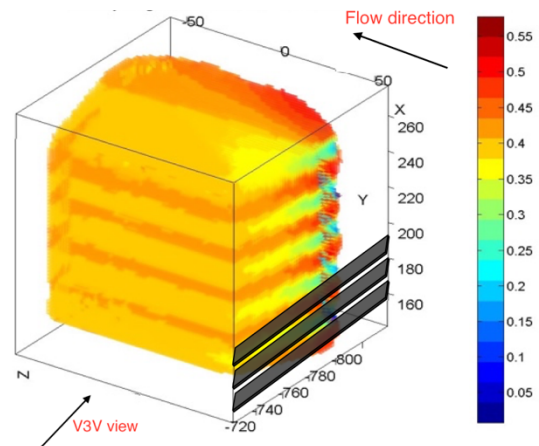


Figure 4.5: Example of V3V isometric velocity plot with horizontal bar placement

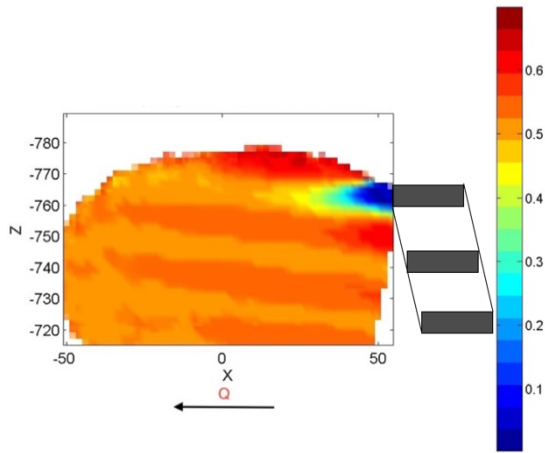


Figure 4.6: Example of top view velocity plot with vertical bar placement

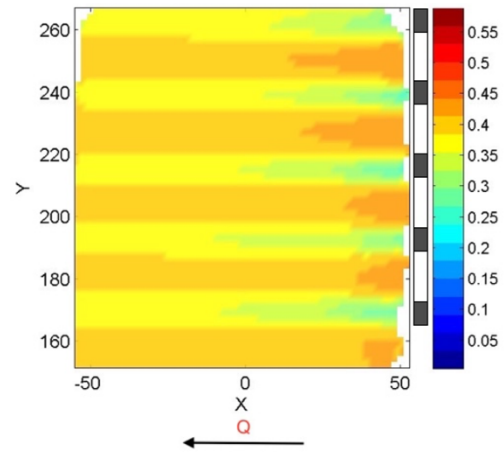


Figure 4.7: Example of side view velocity plot with horizontal bar placement

#### 4.2.1 Downstream measurements

Figure 4.8 shows the velocity magnitude distribution for Rack I-II and Rack V-VI at  $Q = 170$  l/s in an isometric projection. The plots in Figure 4.8 have a patch of low velocities following a column on the far right hand side. This is the region just behind one of the bars, and close to where the measurement volume and the rack intersect. Figure 4.8(b) does not show this region because the measurement volume is reduced in the  $z$ -direction. Figure 4.8 shows that the velocity distribution is consistent with the bar arrangement. The slices of higher velocity are placed at the gaps between the bars, with the slices of lower velocity being right behind the bars. Note that there are no isometric projections of the velocity distribution for Rack III-IV due to the V3V systems limitations discussed in chapter 3.1.4.

Top views of the downstream flow for each rack at  $Q = 170$  l/s can be seen in Figure 4.9. The slices are taken from the middle of each measurement volume along the  $y$ -axis. Figure 4.9(c)-(d) and shows the velocity data obtained by the 2D PIV setup described in chapter 3.1.4. The 2D PIV setup were only used for Rack III-IV. The bar location is represented by the indents in the colour plot. Side views are used when plotting the velocity magnitude distribution for Rack V-VI due to the horizontal bars. A top view will not show the difference in velocity across the bars. Figure 4.9(e)-(f) show these side views. Additional velocity distribution plots for  $Q = 200$  l/s are placed in the Appendix A.

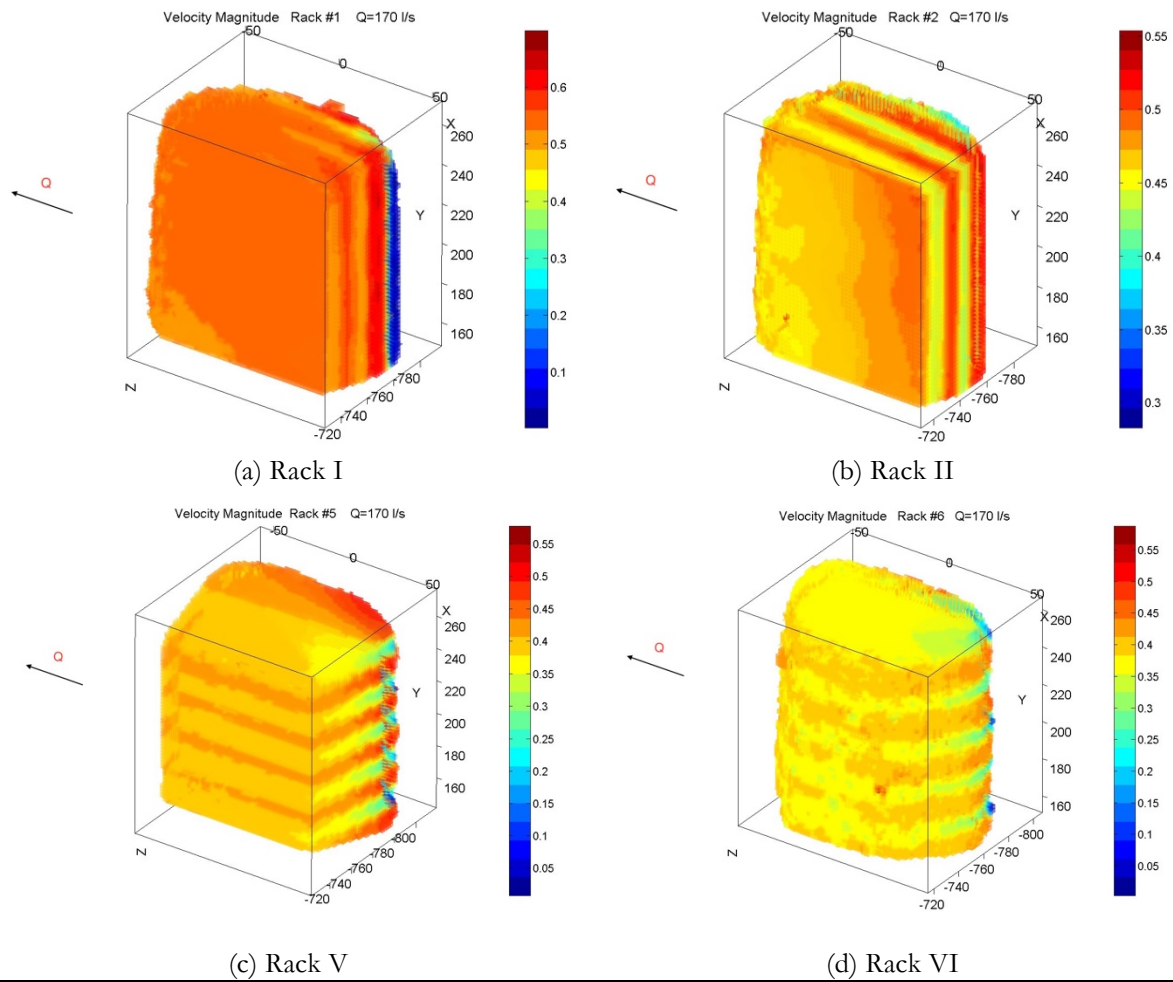


Figure 4.8: Isometric projection of velocity magnitude [m/s] distribution for Rack I-II and Rack V-VI at  $Q = 170$  l/s downstream of the rack

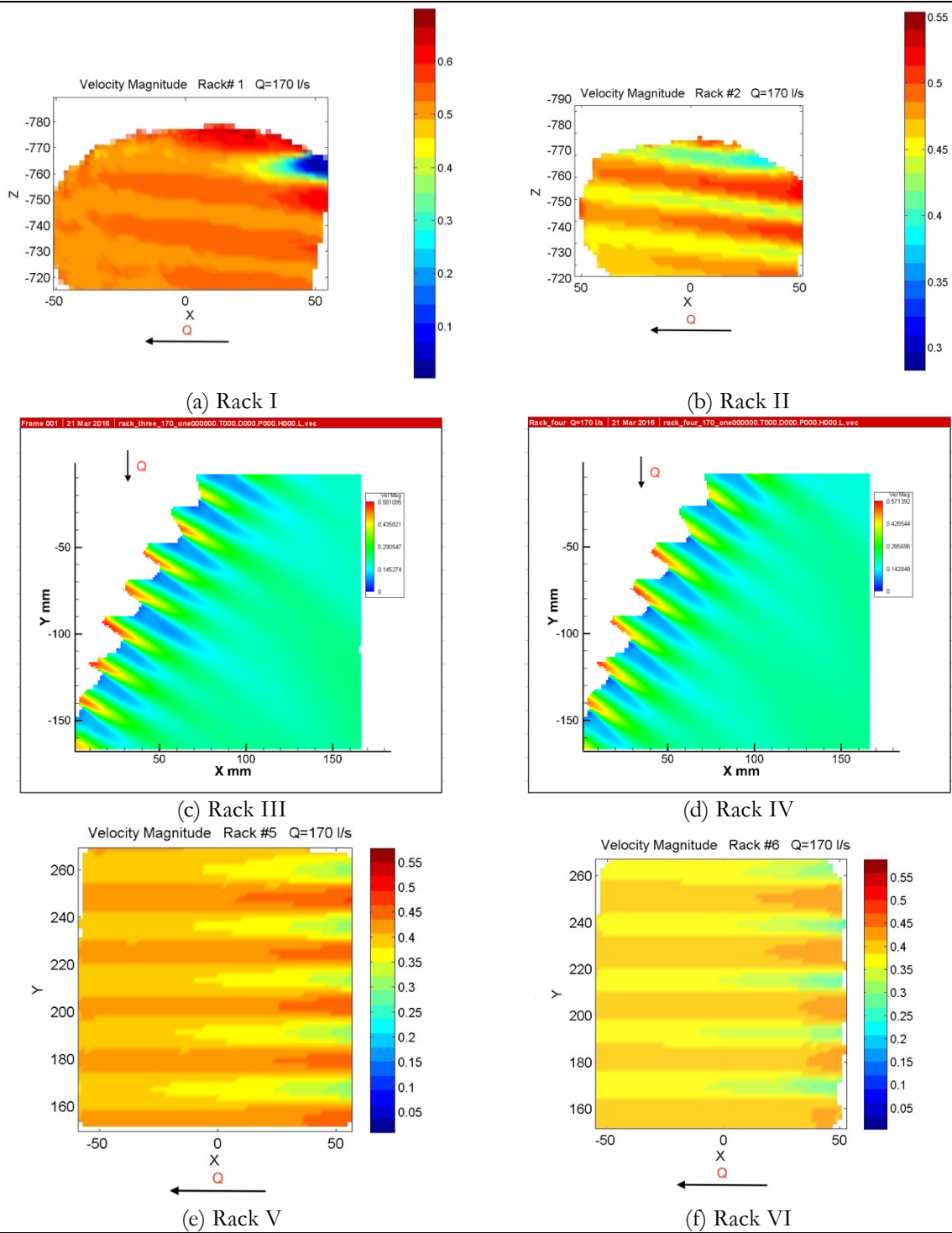


Figure 4.9: Top view velocity magnitude distribution [m/s] for Rack I-IV and front view of Rack V-VI at  $Q = 170$  l/s downstream of the rack

## 4.2.2 Upstream measurements

Figure 4.10 shows the volumetric velocity magnitude distribution for the V3V measurements carried out upstream of the rack. A top view of the middle slice from the same velocity magnitude distribution can be seen Figure 4.11. The reason for picking the middle slice is due to the data in the middle of measurement volumes obtained from the V3V system being typically stronger than the data closer to the edges. The rack placement relative to the upstream measurement plots, and the V3V camera view, are the same as for the downstream plots. Only upstream plots for Rack II, Rack IV and Rack VI were completed in time for this thesis.

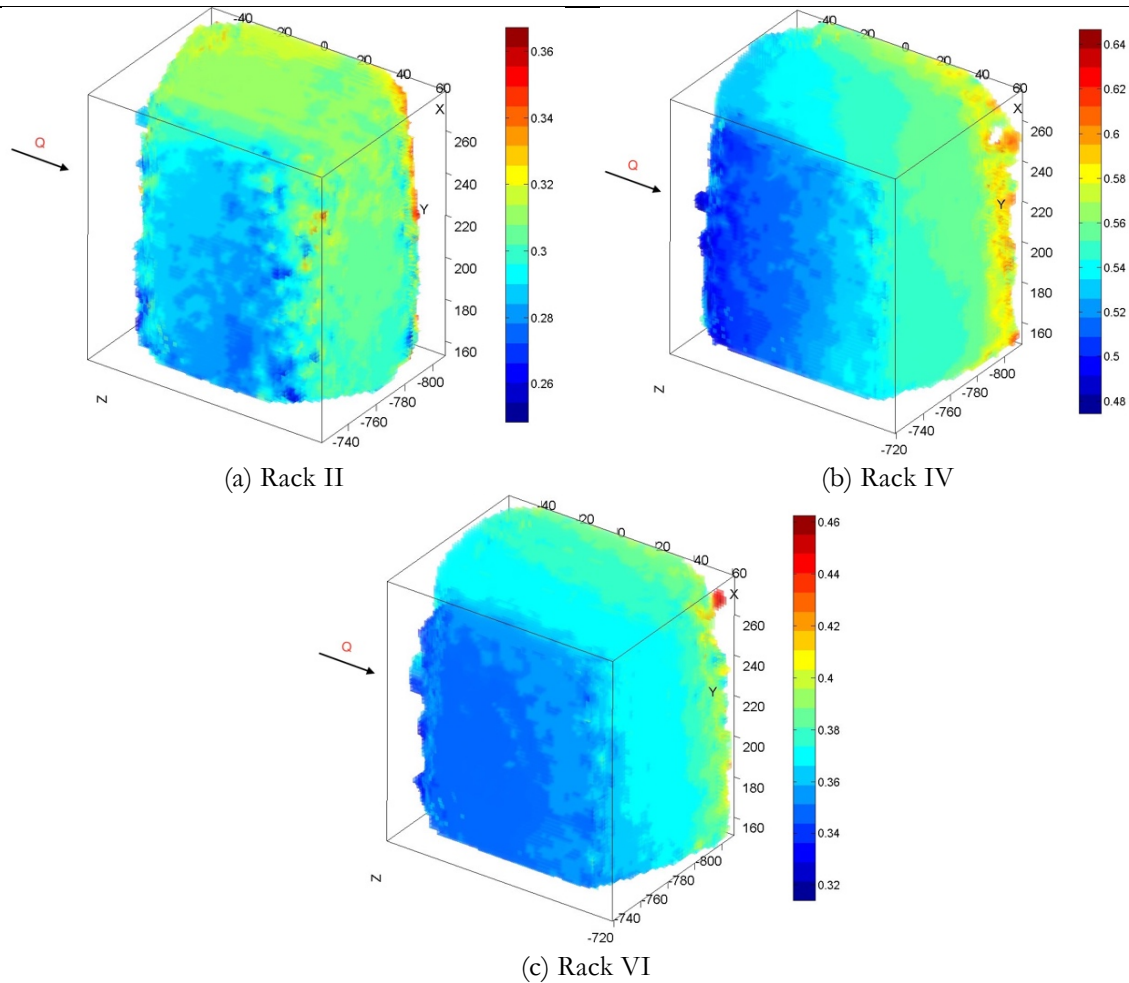


Figure 4.10: Isometric projection of velocity magnitude [m/s] distribution for Rack II, Rack IV and Rack VI at  $Q = 170$  l/s upstream of the rack

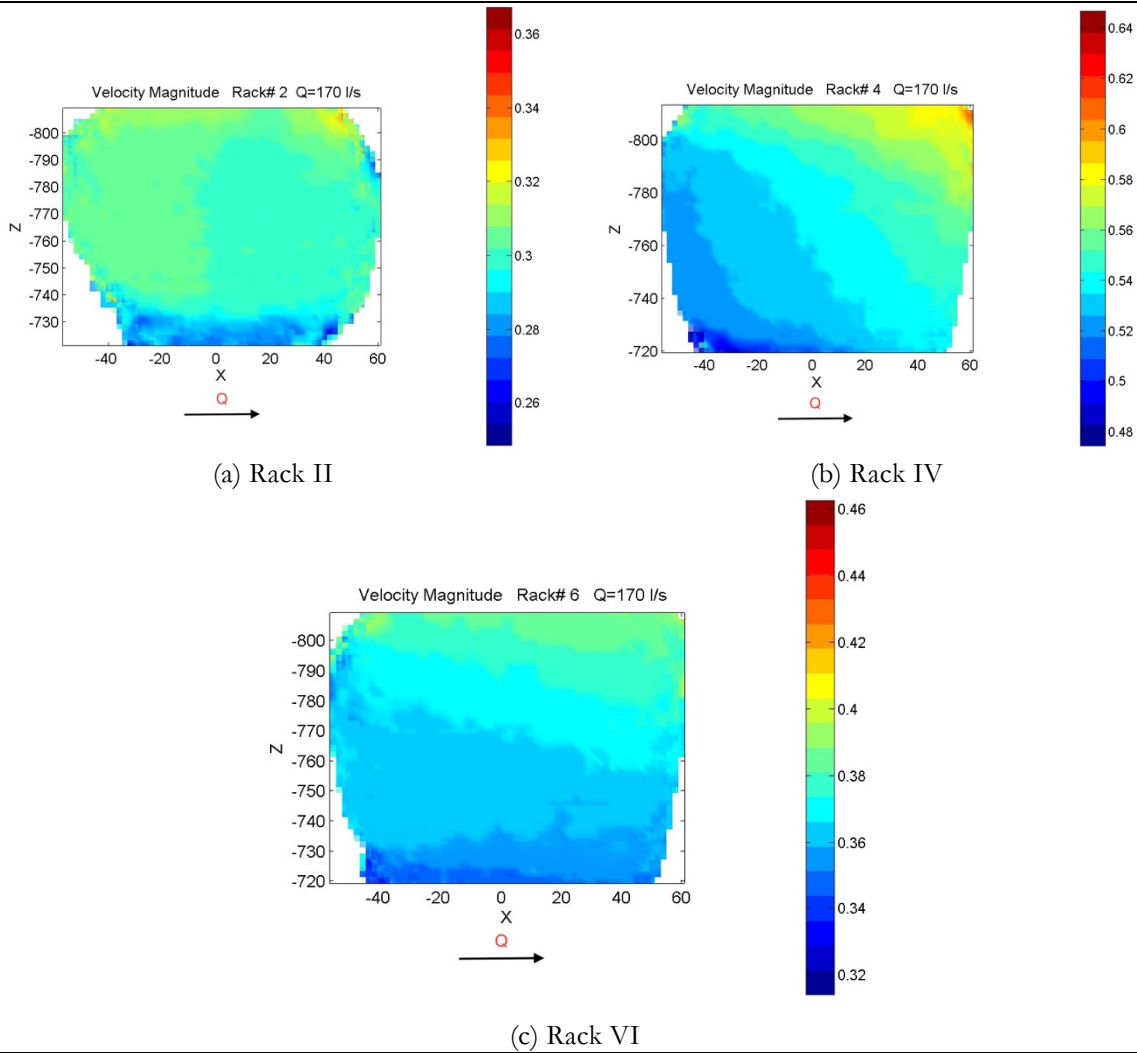


Figure 4.11: Top view velocity magnitude [m/s] distribution for Rack II, Rack IV and Rack VI at  $Q = 170$  l/s upstream of the rack

## 5 Discussion and conclusion

### 5.1 Measured water level and head loss

Figure 4.1 shows that the trash racks with drop shaped bars perform far better than the trash racks with rectangular bars with regards to decrease in hydraulic head. This is in compliance with the thought of profiled and more hydrodynamic bars reducing the wake, and the subsequent energy dissipation.

The water level at Rack I-II increases when approaching the rack, rather than decreasing which is the case for the remaining racks. This suggests that the approaching velocities for Rack III-IV and Rack V-VI are higher than for Rack I-II, hence resulting in a higher velocity head and lower water level. Figure 4.10 and Figure 4.11 shows that Rack I-II have lower approaching velocities than the remaining racks, which indicates that this might be the reason for this discrepancy in approaching water level. Figure 4.1 also shows that the different trends in approaching water level evens out with lower discharges, which again indicates that the differences depend on the approaching velocity.

There is some uncertainty related to the piezometer readings. Based on estimation, the uncertainty linked with the piezometer measurements are  $\pm 1$  mm. Uncertainties are especially high for the measurements downstream of rack, as the water surface was more disturbed than the water surface upstream of the rack. For the velocity calculation the uncertainty has negligible effects as it accounts for less than a percent of the total water level. However, it can have considerable effect on the accuracy of calculated head losses especially at lower discharges. The differences in elevation head are less than 2 mm for all racks at  $Q = 80$  l/s and  $Q = 50$  l/s. As a consequence, the measurements carried out at lower discharges are subject to large errors. For example, the water level measurements for Rack V in Figure 4.1 shows abnormal behaviour at  $Q = 50$  l/s. The measured friction loss due the flume shown in Table 4.1 will also be subject errors at low discharges. Table 4.4 shows that the head losses for Rack I-II and Rack V-VI at the two lowest discharges are far too low to conclude with anything more than that they are almost zero. Rack II at  $Q = 80$  l/s even shows negative head loss. However, lower discharges cause less disturbance of the water surface so it is reasonable to assume that there would be slightly lower uncertainties related to the piezometer measurements. Especially when determining the friction losses caused by the flume.

Table 4.4 and Figure 4.2 shows the calculated head loss based on the piezometer measurements. Rack II and Rack VI creates far less head loss than the remaining racks tested in this experiment. Rack I-II and Rack V-VI all have optimal bar orientation with regards to obstruction of the flow. The flow is not directed off course by the bars it self, resulting in a much calmer passing through the trash racks. This is not the case for Rack III-IV, where the bars have a  $60^\circ$  angle relative to the approaching flow. The bars also have a  $60^\circ$  angle relative to the downstream flow, which leads the flow to be deflected twice resulting in increased energy dissipation. Rack III-VI show the greatest head loss of all racks tested. Even Rack VI, which have drop shaped bars, perform far worse than Rack I and Rack VI which has rectangular bars. This indicates that the orientation of the bars plays a much bigger role for overall head loss than the shape of the bars. Rack V performs considerably better than Rack I, despite Rack V having a slightly higher blockage ratio. This shows that rectangular horizontal bars give less head loss than vertical stream wise rectangular bars. Rack II do however create slightly less head loss than Rack VI. This indicates that horizontal bars are less sensitive to change in bar shape than vertical streamwise bars.

## 5.2 Predicted head loss

The calculated head loss coefficients from the given head loss equations are shown in Table 4.10 with the subsequent calculated head losses at  $Q = 170$  l/s plotted in Figure 4.3. Figures for the remaining discharges can be found in Appendix B. Figure 4.3 and the shows that all head loss equations, except Eq. 2.6 by Raynal et al. (2013b), provide relatively accurate results for Rack I-II and Rack V-VI. For Rack IV the equations do not come close to predicting the head loss, with most being far too low. The same pattern can be seen for Rack III, but Meusburger (2002) and Kirschmer-Mosonyi (1966) show reasonable predictions. This is especially visible at lower discharges.

The predicted head loss by Raynal et al. (2013b) shows no relation with the measured head losses for any of the racks. The predicted head loss values are far higher than the measured head loss for all racks and discharges. Albayrak et al. (2014) argues that Raynal et al. (2013b) does not take into account the orientation of the bars, only the angle of the rack, when predicting the head loss and as a consequence it will yield distorted results. However, Raynal et al. (2013b) implies that the equation is based on experiments where the bar angle is complementary of the rack angle, i.e. bars perpendicular to the axis of the rack. This is however not explicitly stated in the paper. This would suggest that Raynal et al. (2013b) might be able to give accurate values for Rack III-IV, but it greatly overestimates the head loss values for these racks as well. The first thing noticeable from the head loss prediction by Raynal et al. (2013b) is that it predicts higher head loss for racks with drop shaped bars than for rectangular bars. This contradicts the understanding of flow fields around objects like bars in a trash rack. This discrepancy is a result of the bar shape factor  $k_s$ , which is 1.69 for rectangular bars and 2.78 for drop shaped bars. There is a possibility that this is just a misprint in the paper, but predicted head loss with switched bar shape factors still provide greatly overestimated values. It is also worth noticing that the factor accounting for the blockage ratio in Eq. 2.6 shows contradictory behaviour. As the blockage ratio  $O_g$  decreases the factor increases. As a consequence, the predicted head loss coefficient increases with smaller blockage. In view of what is discussed the predicted head losses by Raynal et al. (2013b) will not be included in further discussions regarding the performance of head loss equations.

For Rack I all head loss equations except Raynal et al. (2013b) the predicted head loss fits the measured head loss quite nicely and they all give more or less identical predictions. However, they all underestimate the head loss values. The measured head loss is approximately 30 % higher than the predicted head losses. This might be a result of not factoring in the angle of the rack, however this contradicts the notion of Rack I-II not being affected by  $\alpha$  with regards to head loss (Raynal et al., 2014). The underestimates might suggest that the bypass has a considerable influence on the head loss and the flow pattern around bars, which is not taken into account in the equations. According to the additional head loss plots in Appendix B, the difference in measured and predicted head loss decreases with decreasing total discharge to the point where it is the same. This indicates that the difference is related to the discharge, and perhaps the discharge through the bypass. For  $Q = 50$  l/s the head loss equations overestimate the head loss. However, as mentioned previously in the discussion, the uncertainty related to the piezometer readings for low discharges are arguably too large for the measurements to be relied on.

There is some uncertainty linked to the velocities used in predicting head losses. This is especially the case for Eq. 2.7 proposed by Raynal et al. (2013a). The position of velocity measurement upstream of the rack were not the same for this experiment and the experiment carried out by Raynal et al. (2013a, 2013b). For the remaining equations the water level from piezometer 3, which was approximately 0.2 meters upstream from the rack, was used. For a correct measurement the water level at the rack itself should be obtained. However, it can be questioned

how much influence this difference in position can have as the difference in water level would only be of a few millimetres, relative to a total water level around 0.5 m.

The bar shape factors used in the head loss equation are a source of uncertainty. The bar shape factor used for drop shaped bars in the equations proposed by Meusburger (2002) and Kirschmer-Mosonyi (1966) may not be applicable for the bars used in this experiment. However, the only difference in the bar shape in this experiment and the bar shape used, given by Kirschmer (1926), is the the depth of the bars. The bar depth  $p$  will arguably not influence the predicted head loss, as the bar shape used from Kirschmer (1926) and the bar shape in this experiment both is characterised as long (Osborn, 1968). The bar shape factor used in the equation by Clark et al. (2010) is subject to a large degree of uncertainty. As none of the bar shapes given were similar to the ones used in this experiment, the bar shape factor was chosen based on appearance. However, the bar shape chosen to represent the real bars appears to be more hydrodynamic. This may result in underestimated head loss values, and might be the reason for the low head loss values predicted by the equation proposed by Clark et al. (2010). For the equations by Raynal et al. (2013a, 2013b) this is not a problem as the bars used in their experiment are identical to the ones used in this experiment.

### 5.3 Flow field in the vicinity of the bars

The downstream in plots in Figure 4.8 and Figure 4.9 show clear differences in velocities generated downstream of the racks depending on the bar shape. The even numbered racks, which have drop shaped bars, show a reduction in velocities compared to the racks with rectangular bars. This indicates that the flow past the bars is calmer and produces less turbulence.

In Figure 4.8 and Figure 4.9 Rack I show a vertical column of very low velocity magnitude values. This region is a wake created right behind one of the bars. Unfortunately, this region was not captured by the V3V system for Rack II, making it impossible to compare it with the plot of Rack I. The plots of Rack V and VI show the creation of wakes along the same region. The plot of Rack V shows more of these wakes, which is expected seeing as how Rack V has rectangular bars. The plots of Rack III and IV clearly shows the creation of large wakes behind the bars, and show similar behaviour as the flow shown in Figure 2.2.

Upstream of the bars the approaching velocities are higher for Rack IV and Rack VI, with Rack IV showing the overall highest velocities. This is seen in Figure 4.10 and Figure 4.11. Upstream velocities for Rack IV also show a relatively large increase when moving towards the rack. The velocity increase propagates perpendicular to the orientation of the bars. Upstream velocities for Rack VI also shows this propagating increase, however the angle is not the same. Rack II creates lower upstream velocities and the velocity distribution is more uniform than for Rack IV and Rack VI. The plots also show that the approaching flow at Rack IV exceeds the 0.5 m/s boundary velocity.

## 5.4 Conclusion

The head loss measurements show that Rack II and Rack VI overall perform better than the remaining racks with respect to head loss. Rack III shows the worst performance. The horizontally barred racks create overall the least head loss, as they were less influenced by the bar shape than the racks with vertical streamwise bars. The measured head loss values were as expected, seeing as how the racks with drop shaped bars perform significantly better than its rectangular counterparts. The drop shaped bars reduced the head loss by over 80 %, 15 % and 60% for the racks with streamwise vertical, perpendicular and horizontal bars, respectively. This shows that the overall effect of bar shape decreases with inclined bars. However, this experiment shows that the orientation and the arrangement of the bars has bigger influence on the overall head loss than the bar shape has.

The velocity measurements downstream of the rack showed that Rack III-IV created larger velocities and larger wakes behind the bars, compared to the other racks. This is due to the angle of the bars. The racks with horizontal bars created the lowest velocities downstream of the rack. Upstream velocities show that Rack IV creates approaching flow velocities that exceed the limit of 0.5 m/s. Rack VI creates slightly higher upstream velocities than Rack II, but both show values under 0.5 m/s.

The comparison of predicted and measured head loss show that the equations proposed by Kirschmer-Mosonyi (1966) and Meusburger (2002) provides the best predictions for the head losses measured in this experiment. All equation, except the equation proposed by Raynal et al. (2013b), showed decent predictions for Rack I-II and Rack V-VI. None of the equations were close to predicting the head losses for Rack IV. The equation by Clark et al. (2010) underestimates head loss values for all racks except Rack V. The equation proposed by Raynal et al. (2013b) showed disappointing results, especially considering the similarity between their and this experiment.

Overall, Rack II and Rack VI proves to be fish friendly, they generate low head losses and less turbulent flow around the bars. This shows that horizontally barred racks may be well suited for intake structures. Therefore, further studies into horizontally barred trash racks are recommended. Also, further studies are needed to fully determine the effects of angled trash racks, accompanied by a bypass, on head losses.

## 6 References

- Cedren.no. (2016). CEDREN - SafePass. [online] Available at:  
<http://www.cedren.no/english/Projects/SafePass> [Accessed 9 May 2016].
- Clark, S. P., Tsikata, J. M., & Haresign, M. (2010). Experimental study of energy loss through submerged trashracks. *Journal of Hydraulic Research*, 48(May), 113–118.  
<http://doi.org/10.1080/00221680903566026>
- Courret, D., Larinier, M. (2008). Guide pour la conception de prises d'eau 'ichtyocompatibles' pour les petites cen-trales hydroélectriques. Agence De l'Environnement et de la Maîtrise de l'Energie (ADEME) ([www.onema.fr/IMG/pdf/2008\\_027.pdf](http://www.onema.fr/IMG/pdf/2008_027.pdf)).
- Crowe, C., Elger, D., Williams, B. and Roberson, J. (2010). *Engineering fluid mechanics*. 9th ed. Hoboken, NJ: Wiley.
- Dekker, W. (2003). Did lack of spawners cause the collapse of the European eel, *Anguilla anguilla*?. *Fisheries Manage*, 10(6), pp.365-376.
- EC 2007. Council Regulation (EC) no 1100/2007 of 18 September 2007 establishing measures for the recovery of the stock of European eel. *Official Journal of the European Union* L248: 17–23.
- Ismail Albayrak Lecturer, Carl Robert Kriewitz PhD Student, Willi H. Hager Professor & Robert M. Boes Professor (2014) An experimental study on fish-friendly trashracks: part I & II, *Journal of Hydraulic Research*, 52:1, 144-146, DOI: 10.1080/00221686.2013.876455
- Jenssen, L., Tesaker, E., Lund, S. & Huber, D. (2006). *Inntakshåndboken*. Oslo: NVEs hustrykkeri.
- Kirschmer, O. (1926). *Untersuchungen über den Gefällsverlust an Rechen*, vol. 1. Mitteilungen des hydraulischen Instituts der TH München, Munich, Germany.
- LARINIER, M. and TRAVADE, F. (2002). DOWNSTREAM MIGRATION: PROBLEMS AND FACILITIES. *Bull. Fr. Pêche Piscic.*, (364 supplément), pp.181-207.
- Meusburger, H. (2002). *Energieverluste an Einlaufrechen von Flusskraftwerken*. Zürich: Versuchsanst. für Wasserbau, Hydrologie und Glaziologie.
- Mosonyi, E. (1966). *Wasserkraftwerke, Band I, Niederdruckanlagen*. VDI Verlag, Düsseldorf
- O'Keeffe, N. and Tumpenny, A. (2005). *Screening for intake and outfalls*. Almondsbury: Environment Agency.
- Pothos S, Troolin D, Lai W, Menon R (2009) "V3V – Volumetric Three-Component Velocimetry for 3D Flow Measurements – Main Principle, Theory and Applications," ISGE 2009 Conference, Cluj-Napoca, ROMANIA, May 14–16, 2009.

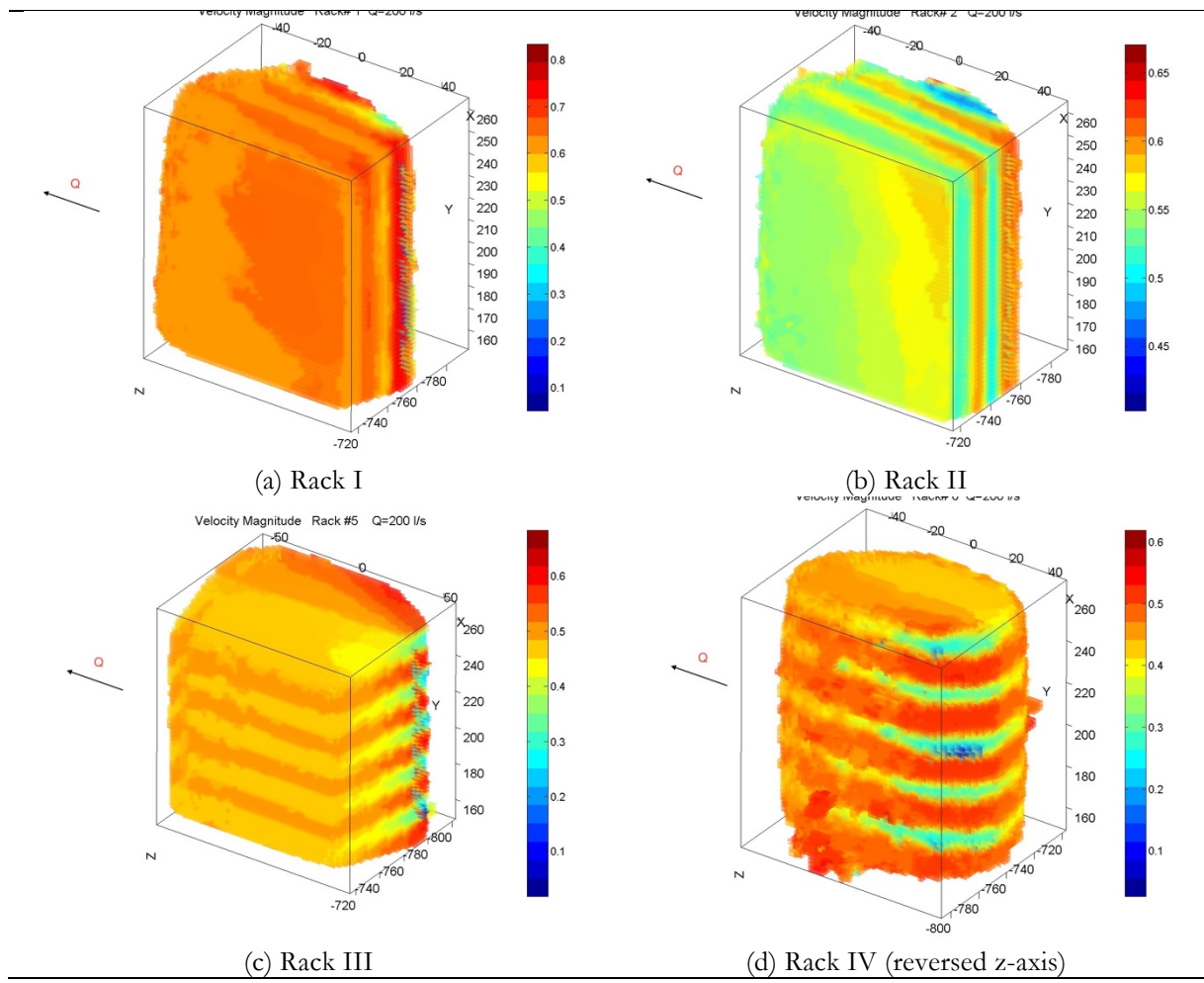
- Raynal, S., Chatellier, L., Courret, D., Larinier, M. and David, L. (2013). An experimental study on fish-friendly trashracks – Part 2. Angled trashracks. *Journal of Hydraulic Research*, 51(1), pp.67-75.
- Rayal, S., Courret, D., Chatellier, L., Larinier, M. and David, L. (2013). An experimental study on fish-friendly trashracks – Part 1. Inclined trashracks. *Journal of Hydraulic Research*, 51(1), pp.56-66.
- Raynal, S., Chatellier, L., Courret, D., Larinier, M. and David, L. (2014). Streamwise bars in fish-friendly angled trashracks. *Journal of Hydraulic Research*, 52(3), pp.426-431.
- Russon, I., Kemp, P. and Calles, O. (2010). Response of downstream migrating adult European eels (*Anguilla anguilla*) to bar racks under experimental conditions. *Ecology of Freshwater Fish*, 19(2), pp.197-205.
- Travade, F., Larinier, M., Subra, S., Gomes, P. and De-Oliveira, E. (2010). Behaviour and passage of European silver eels (*Anguilla anguilla*) at a small hydropower plant during their downstream migration. *Knowledge and Management of Aquatic Ecosystems*, (398), p.01.

# Appendix

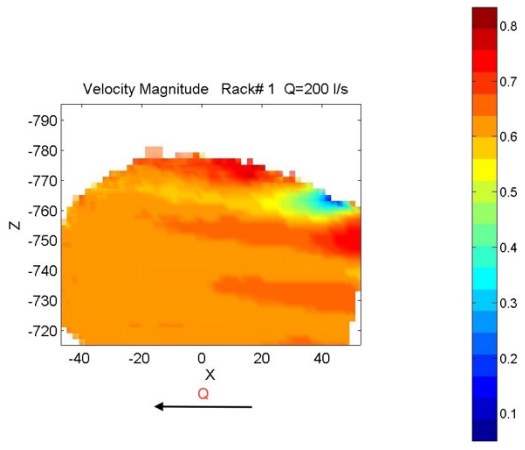
## Table of Contents

APPENDIX A .....	II
APPENDIX B.....	IV

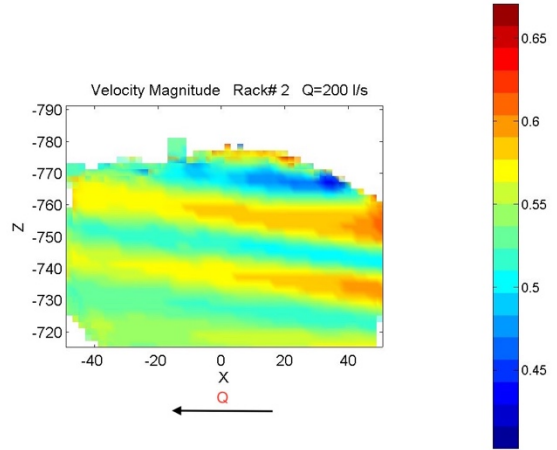
# Appendix A



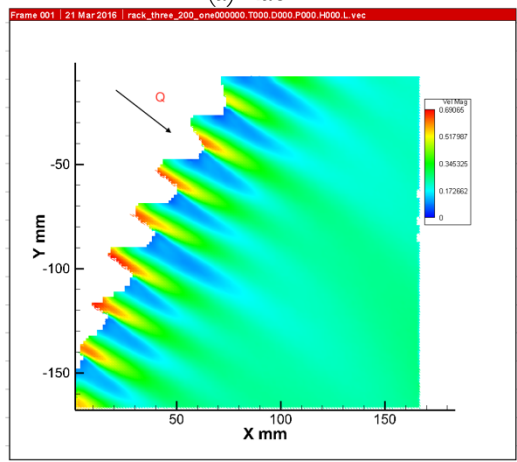
Isometric projection of velocity magnitude distribution for Rack I-II and V-VI at  $Q = 200$  l/s



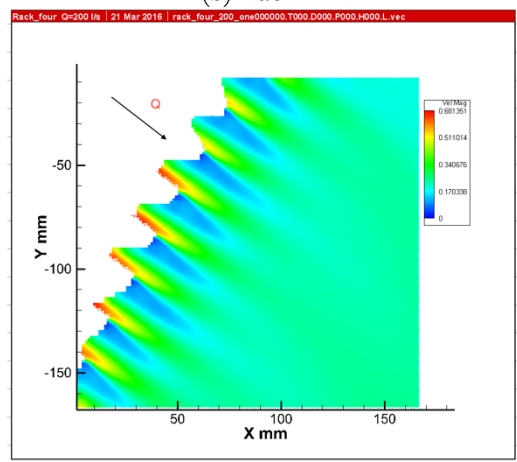
(a) Rack I



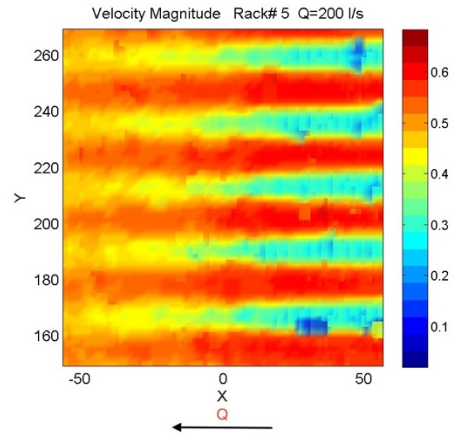
(b) Rack II



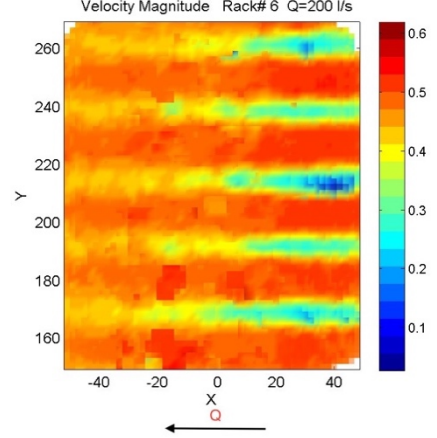
(c) Rack III



(d) Rack IV



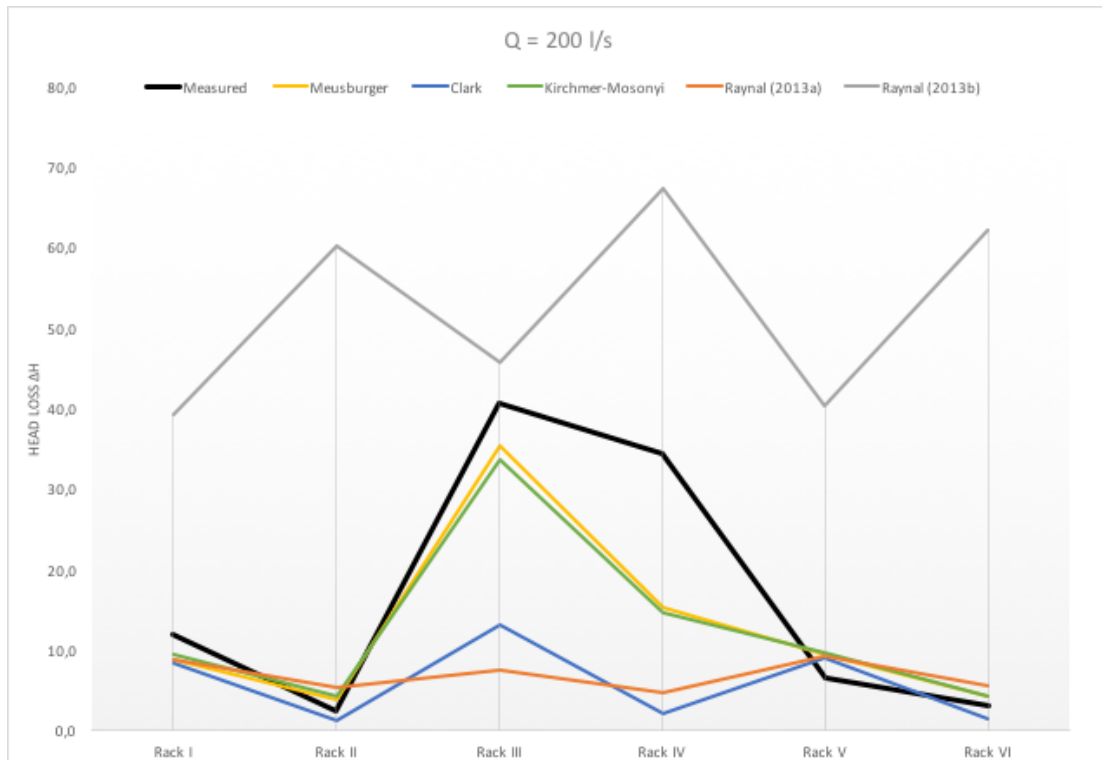
(e) Rack V



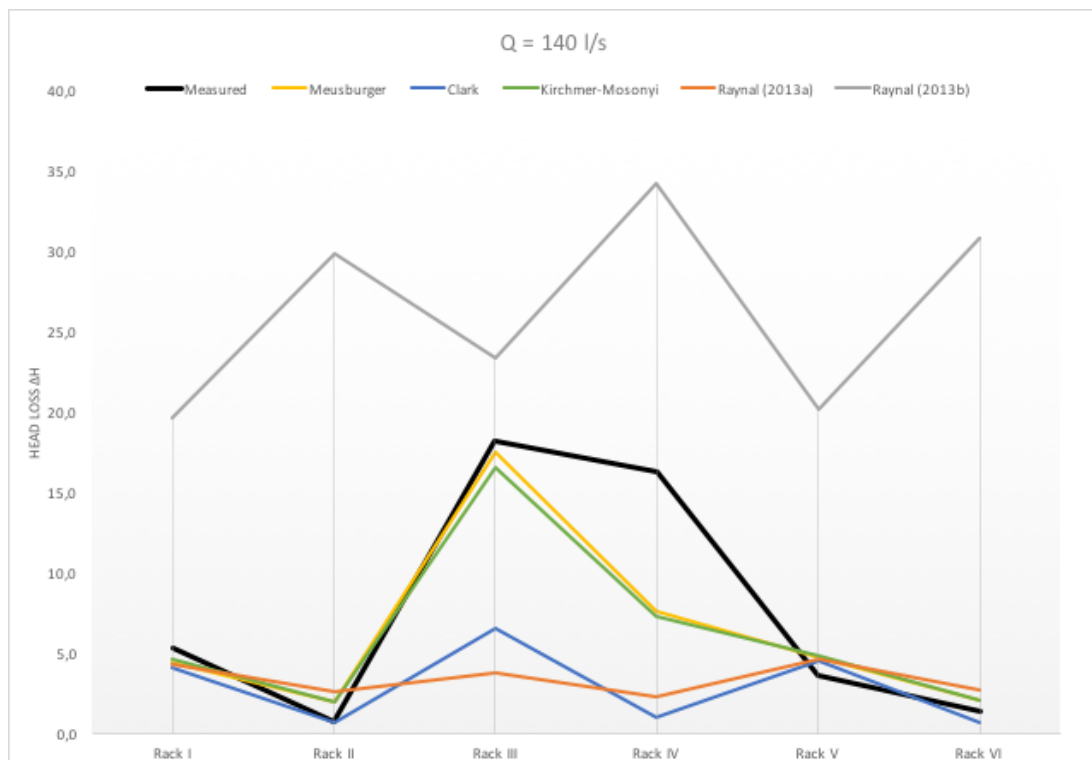
(f) Rack VI

Top view velocity magnitude distribution for Rack I-IV and front view of Rack V-VI at  $Q = 200$  l/s

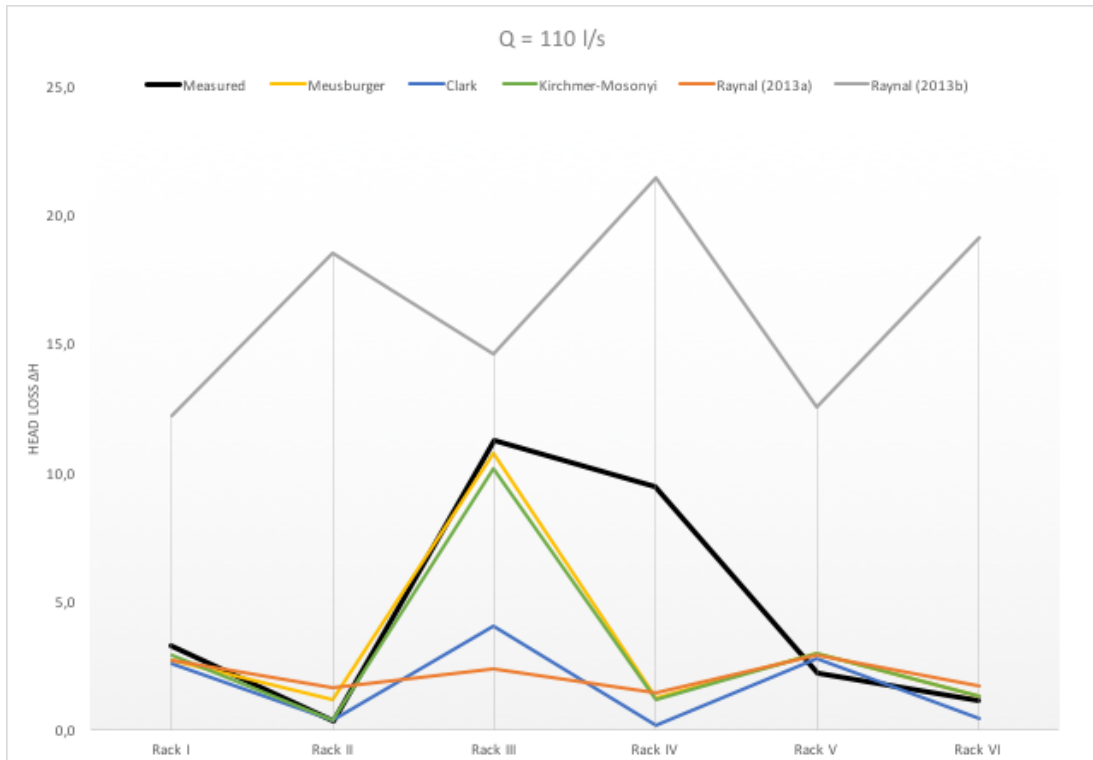
## Appendix B



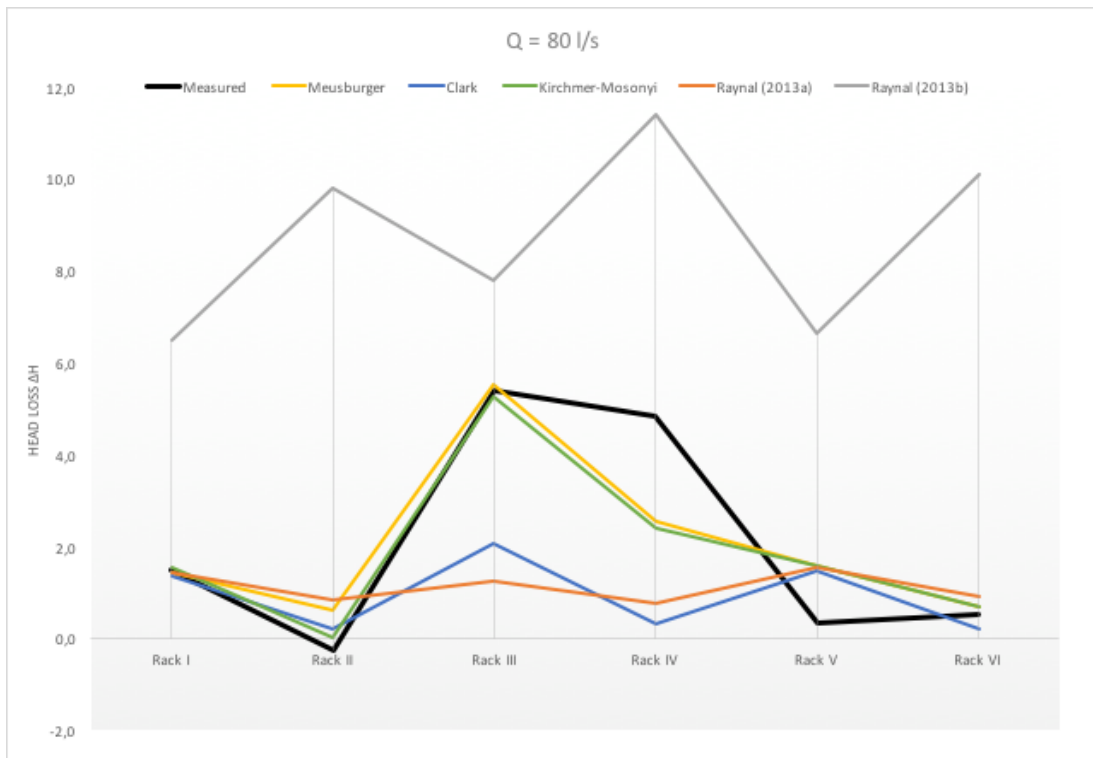
Comparison of predicted and measured head loss  $\Delta h$  at Q = 200 l/s



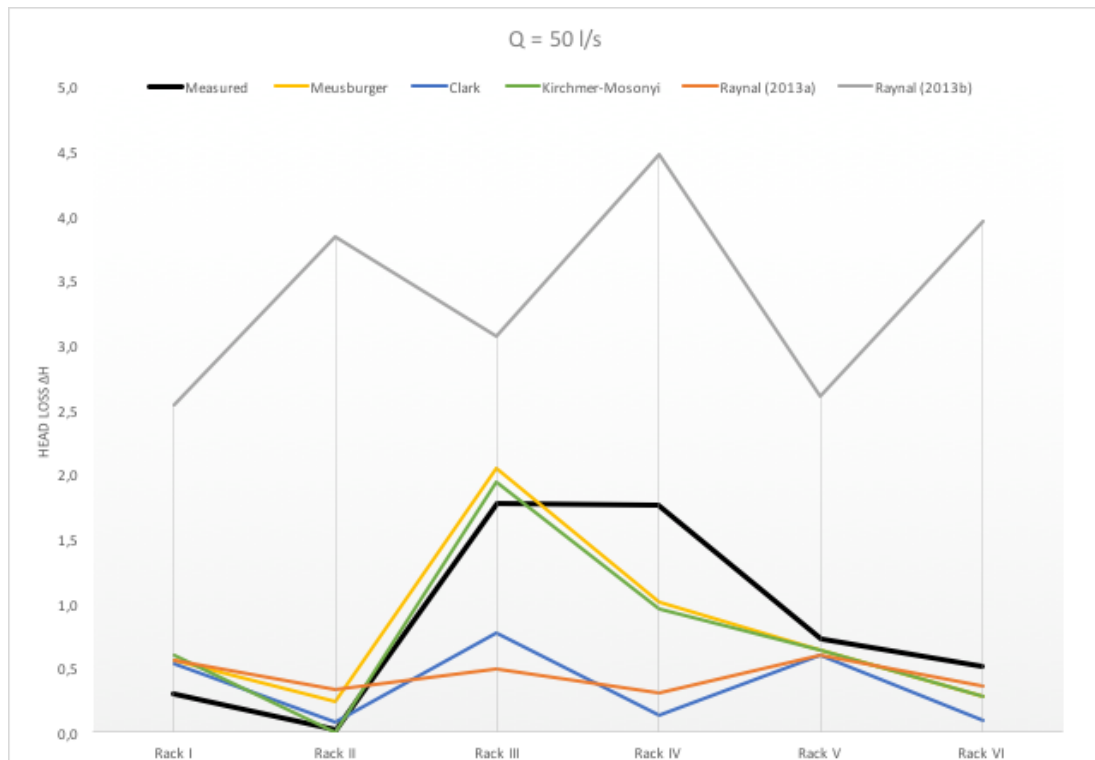
Comparison of predicted and measured head loss  $\Delta h$  at Q = 140 l/s



Comparison of predicted and measured head loss  $\Delta h$  at  $Q = 110$  l/s



Comparison of predicted and measured head loss  $\Delta h$  at  $Q = 80$  l/s



Comparison of predicted and measured head loss  $\Delta h$  at  $Q = 170$  l/s

Q	Rack I	Rack II	Rack III	Rack IV	Rack V	Rack VI
200	0.57	0.47	0.89	0.84	0.47	0.43
170	0.49	0.40	0.73	0.71	0.39	0.37

Velocity measurements [m/s] in the bypass after the ramp

Rack	Q	
	170	200
1	0.138	0.139
2	0.144	0.142
3	0.130	0.119
4	0.131	0.131
5	0.140	0.141
6	0.141	0.142

Water depth [m] in the bypass

<b>Q [l/s]</b>	<b>Rack I</b>	<b>Rack II</b>	<b>Rack III</b>	<b>Rack IV</b>	<b>Rack V</b>	<b>Rack VI</b>
<b>H<sub>2</sub> [mm]</b>						
200	8.92	5.98	19.08	16.64	9.19	5.02
170	6.25	4.45	13.48	12.04	6.31	3.81
140	4.27	3.26	8.56	7.82	4.06	2.61
110	2.58	2.29	5.46	4.28	2.4	1.71
80	1.22	1.29	2.67	2.29	0.96	0.95
50	0.27	0.82	0.91	1	0.79	0.56
<b>H<sub>4</sub> [mm]</b>						
200	-7.64	-0.83	-27.07	-22.88	-1.81	-2.46
170	-5.46	-0.48	-19.39	-15.62	-2.24	-1.25
140	-3.28	0.28	-11.85	-10.71	-1.8	-0.98
110	-1.9	0.7	-6.92	-6.38	-1.12	-0.75
80	-1.1	0.68	-3.48	-3.38	-0.27	-0.46
50	-0.2	0.62	-0.97	-0.93	-0.14	-0.16
<b>H<sub>3</sub> [mm]</b>						
200	10.02	7.32	9.97	7.46	7.47	3.7
170	7.02	5.11	6.46	4.85	5.56	2.97
140	4.73	3.75	3.94	3.34	3.1	1.66
110	3.15	2.54	2.59	1.99	1.9	0.83
80	1.15	1.32	1.35	0.84	0.8	0.48
50	0.35	0.78	0.65	0.27	0.3	0.12

Water levels relative to the starting water level 0.5 m measured at piezometer 2, 3 and 4.